Mon. Not. R. Astron. Soc. **000**, 1–20 (2007) Printed 6 August 2015 (MN LATEX style file v2.2)

The warm molecular gas and dust of Seyfert galaxies: two different phases of accretion?

M. Mezcua[1,2,3], M. A. Prieto[2,3], J.A. Fernández-Ontiveros[4,5], K. Tristram[6], N. Neumayer[7] and J. K. Kotilainen[8]

[1]*Harvard–Smithsonian Center for Astrophysics (CfA), 60 Garden Street, Cambridge, Massachusetts 02138, USA*
[2]*Instituto de Astrofísica de Canarias (IAC), E–38200 La Laguna, Tenerife, Spain*
[3]*Department Astrofísica, Universidad de La Laguna, E-38206 La Laguna, Tenerife, Spain*
[4]*Istituto di Astrofisica e Planetologia Spaziali (INAF-IAPS), Via Fosso del Cavaliere 100, I-00133 Roma, Italy*
[5]*Department Astrofísica, CEI Canarias – Campus Atlántico Tricontinental (ULPGC–ULL), Universidad de La Laguna, E-38206, Spain*
[6]*European Southern Observatory, Alonso de Córdova 3107, Vitacura, Casilla 19001, Santiago de Chile, Chile*
[7]*Max-Planck-Institut für Astronomie, Königstuhl 17, D-69117 Heidelberg, Germany*
[8]*Finnish Centre for Astronomy with ESO (FINCA), University of Turku, Väisäläntie 20, FI-21500 Kaarina, Finland*

ABSTRACT

The distribution of warm molecular gas (1000–3000 K), traced by the near-IR H_2 2.12 μm line, has been imaged with a resolution < 0.5 arcsec in the central 1 kpc of seven nearby Seyfert galaxies. We find that this gas is highly concentrated towards the central 100 pc and that its morphology is often symmetrical. Lanes of warm H_2 gas are observed only in three cases (NGC 1068, NGC 1386 and Circinus) for which the morphology is much wider and extended than the dust filaments. We conclude that there is no one-to-one correlation between dust and warm gas. This indicates that, if the dust filaments and lanes of warm gas are radial streaming motions of fuelling material, they must represent *two different phases of accretion*: the dust filaments represent a colder phase than the gas close to the nucleus (within $\sim$100 pc). We predict that the morphology of the nuclear dust at these scales should resemble that of the cold molecular gas (e.g. CO at 10–40 K), as we show for CenA and NGC 1566 by Atacama Large Millimeter/submillimeter Array (ALMA) observations, whereas the inner H_2 gas traces a much warmer phase of material identified with warmer (40-500 K) molecular gas such as CO(6-5) or HCN (as shown by ALMA for NGC 1068 and NGC 1097). We also find that X-ray heating is the most likely dominant excitation mechanism of the H_2 gas for most sources.

Key words: techniques: high angular resolution – astrometry – galaxies: nuclei – galaxies: Seyfert – infrared: galaxies.

1 INTRODUCTION

Understanding how supermassive black holes (SMBHs) grow and how this is connected to the formation and evolution of their host galaxy is one of the major questions in astrophysics (e.g. see review by Kormendy & Ho 2013). The accretion of gas coming from galactic scales ($\sim$10 kpc) is considered to be the main fuelling mechanism of SMBHs and eventually of active galactic nuclei (AGN). In order to trigger and feed nuclear activity, gas must be transported from kpc scales to a few Schwarzschild radii around the SMBH and lose its large angular momentum. At kpc-scales, galaxy interactions and mergers and large-scale bars have been proposed as the most efficient mechanisms driving gas into the inner kpc region (e.g. Hopkins et al. 2006; Di Matteo et al. 2008; see Combes 2006 and Jogee 2006 for a review). On smaller scales (a few 100 pc), nested bars (Shlosman et al. 1989), nuclear spirals (Maciejewski 2004) and radiation pressure driven inflows (Wada 2012) are proposed mechanisms for driving matter to the centre.

A nuclear spiral produced in a gaseous medium by shocks induced by the large-scale bar may also drive the gas to the central parsecs of the galaxy (e.g. Englmaier & Shlosman 2000; Prieto et al. 2005; Storchi-Bergmann et al. 2007; Davies et al. 2009). Dusty spirals are also a common phenomenon in both Seyfert and "normal" galaxies (Martini et al. 2003), and provide an alternative mechanism for the fuelling process. The presence of nuclear dust filaments connected to kpc-scale dust structures was observed in several Seyfert galaxies (e.g. Malkan et al. 1998; Hunt & Malkan 2004; Prieto et al. 2014), suggesting that these are the channels of inflow of material from the outer parts of the galaxy to the nuclear region. Probing a connection between the dusty filaments and gas distribution at scales of a few 100 pc and AGN feeding has been possible only in a few nearby AGN using high-angular resolution observations of the cold molecular

gas (e.g. García-Burillo et al. 2009; Krips et al. 2011; Combes et al. 2013, 2014) or of warm gas tracers such as the H_2 molecular gas (e.g. Müller Sánchez et al. 2006; Neumayer et al. 2007; Davies et al. 2009; Hicks et al. 2009, 2013; Mazzalay et al. 2013). The latter is usually traced by integral-field spectroscopy (IFU) observations limited to a small instrumental field of view (FoV), often of less than 3 arcsec $\times$ 3 arcsec. For instance, evidence of a close relation between dust and molecular gas has been observed in the Seyfert galaxies NGC 1566 and NGC 1433, for which recent Atacama Large Millimeter/submillimeter Array (ALMA) observations reveal a nuclear spiral of cold CO(3–2) molecular gas that is fuelling the nucleus and is spatially coincident with the dust structures seen at scales $\leqslant$ 400 pc (Combes et al. 2013, 2014). In NGC 4501, the warm H_2 molecular gas traced by VLT/SINFONI[1] within a FoV of 3 arcsec $\times$ 3 arcsec correlates very well with the filamentary dust lanes observed at scales $<$100 pc (Mazzalay et al. 2013). It should be noted though that kinematic studies of the molecular warm gas provide controversial results concerning the presence of molecular outflows in the central regions of some AGN, as is the case of NGC 1068, for which the results of the SINFONI observations were interpreted as an inflow of warm H_2 gas towards the nucleus at scales of a few pc that could be fuelling the AGN (Müller Sánchez et al. 2009) but as an outflow by Barbosa et al. (2014). Unfortunately, the small FoV of IFU observations is in many cases insufficient to fully characterize the gas kinematics as a large fraction of gas may reside outside the covered IFU FoV, as it is shown in this work.

In this paper we show the full extension of the warm ($\sim$1000-3000 K) H_2 gas of a nearby sample of five type 2 Seyfert galaxies (CenA, Circinus, NGC 1068, NGC 1386 and NGC 7582), one type 1.5 Seyfert (NGC 1566) and one type 1 LINER/Seyfert (NGC 1097), finding that the warm molecular gas is often detached from the central dust lanes and filaments that are observed at equivalent angular scales as the H_2 gas ($\sim$ 0.1–0.4 arcsec). This may be pointing to two modes of accretion: a cold mode, traced by the dust filaments, and a warm mode, traced by the warm H_2 gas and warm molecules such as HCN or CO of high J levels traced by ALMA. The existence of two distinct accretion modes, hot (10^{5-6} K) and cold, has been shown by observations (e.g. Hlavacek-Larrondo et al. 2013), predicted by high-resolution simulations of black hole accretion on sub-kpc scales (e.g. Gaspari et al. 2013; Bourne et al. 2014) and implemented in cosmological simulations by Steinborn et al. (2015) in an attempt to better describe a smooth transition between the so-called radio- and quasar-modes of accretion. The existence of an intermediate warm gas mode of accretion should therefore take place. We tackle this aspect in this paper by investigating the association between relatively warm ($\sim$1000-3000 K) H_2 gas and cold dust filaments seen in detail in the central few 100 pc of active galaxies. The targets have been drawn from a larger sample that includes the nearest and brightest AGN that could be observed at high resolution in the infrared (IR) using the VLT and adaptive optics (AO; Prieto et al. 2010; Reunanen et al. 2010). We present near-IR narrow-band H_2 imaging observations with the VLT of this sample of seven nearby AGN. The large FoV of the observations (up to 26 arcsec $\times$ 26 arcsec) and high spatial resolution (down to 0.1 arcsec) allows us to study the distribution of the molecular H_2 warm gas and its potential as a tracer of dust at scales from a few tens of pc to a few 100 pc as well as to estimate the amount of gas available for accretion on to the SMBH. In addition to the narrow-band imaging data, we present near-IR broad-band imaging data taken with the same instrument, optical I- and V-band data from the *Hubble Space Telescope* (*HST*), AO VLT/SINFONI data, X-ray imaging data from the *Chandra* X-ray satellite, and CO and HCN intensity maps from ALMA.

The paper is organized as follows. The observations and data reduction are presented in Section 2. The data analysis is described in Section 3. The results obtained are presented and discussed in Section 4, while final conclusions are summarized in Section 5. An individual description of each target galaxy is provided in Appendix A.

2 OBSERVATIONS AND DATA REDUCTION

2.1 Adaptive optics IR data

The seven galaxies listed in Table 1 were observed with the near-IR AO assisted instrument Naos-Conica (NaCo; Rousset et al. 2003) installed at the Nasmyth focus on ESO VLT (Paranal, Chile). Near-IR images in several broad- and narrow-band filters in the K-band were taken with NaCo using the pixel scale of 0.027 arcsec pixel^{-1}. A FoV of 26 arcsec $\times$ 26 arcsec of the central few 100 pc was covered by NaCo for all the galaxies. In all cases the AO correction was done on the nucleus or a star cluster close to the nucleus using wavefront sensing in the optical. For the purpose of this paper, we make use of the 2 μm broad-band *Ks* filter ($\lambda_c = 2.180$ μm, $\Delta\lambda = 0.350$ μm) to obtain the continuum image. This should provide the maximum contrast between the nuclear emission and the host galaxy (e.g. Prieto et al. 2010, 2014).

For all the targets, narrow-band images were taken with two filters, each with different width but both centred on the H_2 1–0 S(1) 2.12 μm line. The filters used were NB2.12 (width 0.022 μm) and IB2.12 (0.06 μm). Exposure time in both filters was the same for each galaxy, ranging from 4 to 5 min on-source. Since the seven target galaxies are nearby and have small systemic velocities (see Table 1), the H_2 1–0 S(1) 2.12 μm line is fully covered by the NB2.12 filter. The resolution in these narrow-band images was estimated from point-like sources detected in the FoV. In NGC 1566 foreground stars were used for resolution estimate, while for the rest the estimate was based on stellar clusters, which are unresolved with 8-m telescopes in the near-IR. For each galaxy, the spatial resolution achieved in the two filters is comparable and ranges from full width at half maximum (FWHM)$\sim$0.12 arcsec for NGC 1566 to FWHM$\sim$0.35 arcsec for NGC 1097 (see Table 1).

For the galaxies Cen A, Circinus and NGC 1386, the intermediate-band line-free filter IB2.06 ($\lambda_c = 2.060$ μm, $\Delta\lambda = 0.060$ μm) was also used to estimate the continuum level.

The NaCo data reduction was performed following the standard procedure of sky-subtraction, flat fielding and combination of frames with the ESO ECLIPSE package (Devillard 1999).

The imaging data are complemented with IFU VLT/SINFONI data for NGC 1386, NGC 1566 and NGC 7582. The data reduction was performed using the SINFONI pipeline provided by ESO and includes: correction for bad pixels, flat-field, geometric distortions, wavelength calibration, reconstruction of the data cube from the image spectral slices, background subtraction using sky frames, and flux calibration using a standard star.

[1] Spectrograph for INtegral Field Observations in the Near Infrared (SINFONI) on the Very Large Telescope (VLT).

Table 1. Galaxy properties, filters and errors.

Object	Galaxy type	AGN type	L_{bol} [erg s^{-1}]	D_L [Mpc]	Linear scale [pc arcsec^{-1}]	Ref.	Dust map filters	H_2 gas filters	FWHM *Ks*	FWHM NB2.12	Clusters registration	Errors registration [mas]
(1)	(2)	(3)	(4)	(5)	(6)	(7)	(8)	(9)	(10)	(11)	(12)	(13)
CenA	S0	Sy2	6×10^{42}	3.8	17	[1]	K/F814W	NB2.12-IB2.12	0.″12	0.″13	4*	60, 120, 60, 70
Circinus	SAb	Sy2	8.4×10^{42}	4.2	19	[2]	K/F814W	NB2.12-IB2.12	0.″16	0.″16	3	40, 30, 30
NGC 1068	Sb	Sy2	8.7×10^{43}	14.1	70	[3]	K/F550M	NB2.12-IB2.12	0.″14	0.″13	3	30, 30, 10
NGC 1097	SBb	L1/Sy1	1.5×10^{41}	14.2	69	[4]	K/F814W	NB2.12-IB2.12	0.″14	0.″35	7	20,30,30,30,20,30,30
NGC 1386	SBa	Sy2	1.2×10^{42}	15.3	74	[5]	K/F814W	NB2.12-IB2.12	0.″09	0.″19	2*	10, 10
NGC 1566	SABbc	Sy1.5	5.5×10^{42}	20.5	99	[6]	K/F438W	NB2.12-IB2.12	0.″13	0.″12	3	40, 40, 10
NGC 7582	SBab	Sy2	1.8×10^{43}	19.9	96	[7]	F160W/F606W	SINFONI**	0.″16	0.″24	4	20, 50, 70, 20

Column designation: (1) Object name; (2) galaxy type; (3) AGN type: Sy stands for Seyfert, L for LINER; (4) bolometric luminosity, from Mezcua & Prieto (2014) and Prieto et al. (2010); (5) luminosity distance; (6) linear scale; (7) references for column (5): [1] Harris et al. (2010); [2] Freeman et al. (1977); [3] Marco et al. (1997); [4] Tully et al. (2009); [5] Jensen et al. (2003); [6] NED adopting H_0 = 73 km s^{-1} Mpc^{-1}; [7] Terry et al. (2002); (8) and (9) filters used to construct the dust maps and H_2 gas maps, respectively; (10) and (11) FWHM of the *Ks*-band and NB2.12 filters; (12) number of stars/clusters used in the alignment; (13) error on the position of each star/cluster used in the alignment.
* for CenA and NGC 1386, the NB2.12 and IB2.12 images have been aligned to the NaCo/*K*-band image using the nucleus; ** for NGC 7582 no good quality map with NaCo is available. The H_2 molecular gas map of this galaxy is thus derived from SINFONI data.

2.2 *HST* optical data

To construct the colour dust maps, we searched in the *HST* archive for the reddest image available for each galaxy. This should provide the largest number of common sources to the 2 μm NaCo images to use as reference sources in the image registration. Broad *I*-band images corresponding to the *HST/F814W* filter from either the WFPC2[2] or the WFC3[3] cameras were retrieved for most of the target galaxies (see Table 1). When not available, the *V*-band image from the ACS/*F550M* filter was used. In the case of NGC 7582, the colour maps were built using the WFPC2/*F606W* and NICMOS[4]/*F160W* images to avoid the strong contribution of the nucleus in the *K*-band. In all cases the pixel scale ranges from 0.04 to 0.05 arcsec pixel^{-1}.

For data sets with multiple exposures, the retrieved images were combined and corrected for geometric distortions using the *MultiDrizzle* package in PyRAF (Koekemoer et al. 2003). Cosmic rays removal was applied for those datasets with single exposures using the L.A. Cosmic algorithm (van Dokkum 2001) in its *Python* module version[5]. Further analysis was performed with IRAF/PyRAF.

3 ANALYSIS

3.1 Extraction of H_2-line maps

The extraction of the continuum-free H_2 images was performed in two steps. First, the subtraction of the two images centred on the 2.12 μm H_2 line (IB2.12–NB2.12) produced a pure continuum (offline) image. This pure-continuum image was further used to extract pure H_2 images from the narrow-band NB2.12 image using a scaling factor. This process was repeated iteratively, changing the scaling factor, until the residuals of the H_2 emission-line image were smooth. Effectively this corresponds to $H_2 = NB - c \times (IB - NB)$, where c is the scaling factor. This process was performed to obtain the H_2 maps of all the galaxies in the sample except for NGC 7582 (see below).

For Cen A, Circinus and NGC 1386, H_2 maps were also extracted using the filters IB2.12 and IB2.06, containing the emission line and adjacent continuum, respectively. A similar iterative process was applied to extract the H_2 emission-line maps. The latter were compared to those based on the NB2.12 filter. In all cases, similar H_2 structures are derived using these two approaches.

In addition to the NaCo narrow-band imaging, we show for all sources (Figs. 3-9) the molecular H_2 gas distribution obtained from AO VLT/SINFONI IFU observations. For Cen A, NGC 1068, NGC 1097, NGC 1386 and NGC 1566, the H2 line maps have been extracted from the SINFONI data cube using QFITSVIEW[6]. The 3D data cube allows an optimized extraction of the line emission, subtracting the adjacent continuum measured at both sides of the line. The warm SINFONI H_2 maps for Circinus and NGC 1068 are directly from Müller Sánchez et al. (2006) and Müller Sánchez et al. (2009), respectively.

For NGC 7582, the IB2.06 filter could not be used as reference for the continuum level due to contamination from the He I emission line at 2.058 μm, associated with the circumnuclear starburst. Thus, the H_2 line map shown in Fig. 9 was extracted from the SINFONI data cube following the same procedure as for CenA, NGC 1097, NGC 1386 and NGC 1566.

3.2 Image registration

For each target galaxy, the *HST* images were registered to the NaCo *K*-band image and the H_2 narrow-band images using at least two point-like reference sources (usually unresolved stellar clusters in the galaxy and avoiding the nucleus when possible) in the common FoV to all images. In general, up to three to four reference sources could be identified (see Table 1) due to the limited FoV and the strong galaxy emission in the near-IR. The image registration was performed with the IRAF task *imalign* and crosschecked with an alignment script written by us in IDL[7] following the same procedure as in Prieto et al. (2014). The relative offsets between the images were determined using the centroid position of the reference

[2] Wide-Field Planetary Camera 2.
[3] Wide-Field Camera 3.
[4] Near Infrared Camera and Multi-Object Spectrometer.
[5] http://python.org
http://obswww.unige.ch/~tewes/cosmics_dot_py/

[6] http://www.mpe.mpg.de/~ott/QFitsView/
[7] Interactive Data Language.

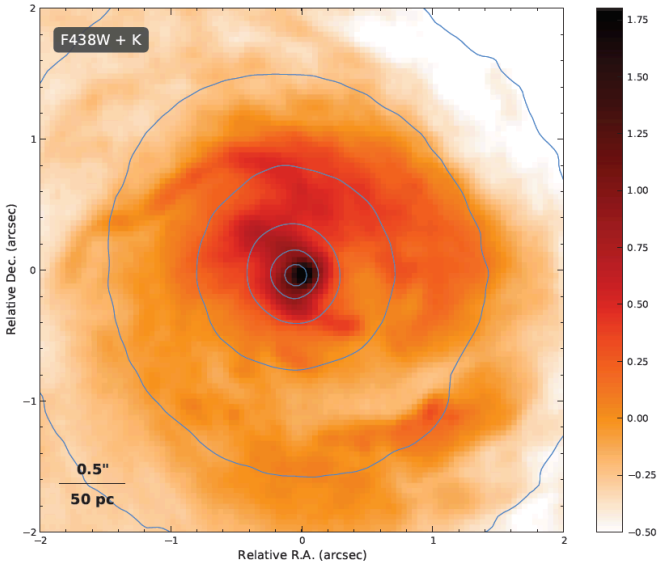

Figure 1. NGC 1566. *HST/F438W* image with NaCo/*K*-band continuum contours in blue. The FoV is 4 arcsec × 4 arcsec. The colour scale is in arbitrary units. North is up and east is to the left.

sources identified in the common FoV and never using the nucleus to register the near-IR and optical images (see Prieto et al. 2014). The near-IR nucleus was only used to align the *K*-band image to the H_2 narrow-band image in the case of CenA, NGC 1386 and SINFONI for NGC 7582. The average of these offsets was used to shift and align the images. For each target, the alignment error of each reference source is estimated as the standard deviation of its position in the different images (Table 1, column 13). The mean of these individual errors is taken as the final error of the alignment for each target galaxy, which ranges between 20 and 80 mas. Therefore, any uncorrected distortions or wavelength-dependent effects affecting the centroid position of the point-like reference sources used in the image registration are accounted for in the final alignment error. See Prieto et al. (2014) for further details.

The accurate registration of the *Ks*-band and *HST* optical images allows us to confirm the shift between the *HST/F814W* and NaCo/*Ks*-band peaks previously reported for the type 2 Seyfert Circinus and to constrain it to 160 ± 30 mas (Mezcua et al., in preparation). For the same galaxy we also note a shift of 40 ± 30 mas between the peak of the warm H_2 molecular gas and the *Ks*-band peak. In addition, we report for the first time an offset between the optical (*HST/F438W*) and NaCo/*Ks*-band peaks of emission for the type 1.5 Seyfert NGC 1566 of 50±30 mas (Fig. 1).

The NaCo warm molecular H_2 gas emission map of Circinus, NGC 1097, NGC 1386 and NGC 7581 has been also aligned to their archival broad-band X-ray *Chandra* image (bottom right panel in Figs. 4, 6, 7, and 9). The image registration has been performed by matching the position of the H_2 peak to that of the nuclear X-ray peak due to the lack of point-like references sources in the common FoV of the H_2 and *Chandra* images. In the case of NGC 1068, the SINFONI warm H_2 gas map has been aligned to the *Chandra* High Resolution Camera (HRC) image of the nuclear region of NGC 1068 (Wang et al. 2012) by matching the position of the nucleus in the *Ks*-band to the nuclear X-ray peak (Fig. 5, middle right panel). This same procedure (i.e. matching the position of the nucleus) has been performed to align the SINFONI warm H_2 gas map of NGC 1068 to its ALMA CO(6-5) map (García-Burillo et al. 2014) and the NaCo warm molecular H_2 gas emission image of NGC 1097, NGC 1566 and CenA to their ALMA HCN (Izumi et al. 2013; Martín et al. 2015), CO(3-2) (Combes et al. 2014) and CO(2-1) maps (Espada 2013), respectively.

3.3 Dust maps

I - *K* or *V* - *K* colour maps of the central few 100 pc of each target galaxy were constructed using the ratio between the aligned NaCo *K*-band and *HST* optical images (Figs. 3–9). These maps show the presence of dust in the central few 100 pc of each galaxy. The dust morphology is in general filamentary, in some cases more disc-like or with irregular shape. In Cen A, Circinus, NGC 1068, NGC 1386 and NGC 7582 (i.e. those type 2 Seyferts) a filament of dust is observed to cross the nucleus, unequivocally identified as an outstanding point-like source in the NaCo 2 µm *Ks*-band images (e.g. Prieto et al. 2010, 2014; Fernández-Ontiveros et al. 2012). Such a nuclear dust lane is not observed in NGC 1566 (Sy1.5) nor NGC 1097 (Sy1). In NGC 1097 the dust is observed to spiral around the nucleus and to recover the same morphology, although with much larger contrast, as that originally discovered in the high-angular resolution *J*-*K* maps of Prieto et al. (2005). In some sources (e.g. NGC 1386) the central dust filaments extend to ∼ 1 kpc and are thus associated with the large-scale dust structure of the galaxies (see also Prieto et al. 2014).

For CenA, NGC 1068, NGC 1386 and NGC 1566 the warm molecular H_2 gas emission map from SINFONI has been aligned to the dust map by matching the position of the H_2 peak to that of the nucleus (or NaCo/*K*-band peak; e.g. Müller Sánchez et al. 2009). All maps are centred at the *K*-band peak and are shown in Figs. 3–9.

3.4 Molecular H_2 warm gas light profile

To quantify the extent of the nuclear H_2 warm gas distribution traced by NaCo, circular or elliptical isophotes were fitted to the central regions of the H_2 emission-line images (i.e. we exclude the H_2 clumps associated with star formation observed in the spiral arms of NGC 1097 or the extended starburst of NGC 7582). The extent of these isophotes, taken as three times the background noise level (σ) of each H_2 emission-line image, is reported in Table 2 (see also Fig. 2). A Sérsic function (Sersic 1968) was fitted to the light profiles of the warm H_2 gas shown Fig. 2.

4 RESULTS AND DISCUSSION

4.1 Morphology of the molecular H_2 warm gas

Molecular H_2 warm gas emission is seen in the central regions of all the galaxies discussed in this paper (see Figs. 3–9). The emission is resolved by NaCo in all cases, and its morphology is varied, ranging from symmetric emission to showing extended filaments. In some cases, the warm H_2 gas is also observed as clumps of emission in the outermost spiral arms (e.g. NGC 1097, see Fig. 6). The gas is thus observed when it is close enough to the nucleus as to be heated by the AGN, though it is equally detected when heated by star-forming regions (also visible in our NaCo *K*-band images). A circular aperture was able to reproduce the morphology of the molecular H_2 warm gas for all sources except for NGC 1386 and NGC 1068, for which an elliptical aperture was found to better reproduce the observed morphology. In the case

Table 2. Properties of the molecular H_2 gas.

Object	Radius		L_{H2}	HWHM	M_{warm}	M_{cold}	N_{cold}	L_{X-rays}
	[arcsec]	[pc]	[erg s^{-1}]	[pc]	[M$_\odot$]	[M$_\odot$]	[cm^{-3}]	[erg s^{-1}]
(1)	(2)	(3)	(4)	(5)	(6)	(7)	(8)	(9)
CenA	2.0	34	2.4×10^{37}	3	50	7×10^{6}	9×10^{3}	1.1×10^{42}
Circinus*	1.4	26	3.9×10^{37}	4	40	1×10^{7}	3×10^{4}	4.3×10^{41}
NGC 1068†	1.5	106	1.7×10^{39}	10	1000	5×10^{8}	6×10^{4}	6.5×10^{41}
NGC 1097*	2.0	138	1.3×10^{39}	29	600	4×10^{8}	6×10^{4}	5.2×10^{40}
NGC 1386†	4.3	321	1.8×10^{39}	100	1000	6×10^{8}	5×10^{4}	1.3×10^{40}
NGC 1566	2.2	220	4.5×10^{39}	27	3000	1×10^{9}	6×10^{3}	3.7×10^{42}
NGC 7582*,††	0.3	29	1.6×10^{38}	14	100	5×10^{7}	1×10^{5}	4.5×10^{42}

Column designation: (1) Object name; (2, 3) aperture radius used to extract the flux of the warm H_2 molecular gas, in arcsec and pc respectively; (4) luminosity of the warm H_2 molecular gas; (5) HWHM of the Sérsic funcion fit to the warm H_2 gas distribution; (6) mass of the warm H_2 molecular gas; (7) mass of the total (cold) H_2 molecular gas; (8) density of the total (cold) H_2 molecular gas assuming a gas-to-mass ratio f_g = 1% for NGC 1097 and f_g = 10% for the rest; (9) X-ray luminosity from the highest energy range available in the literature for CenA, Circinus, NGC 1068, NGC 1097, NGC 1566, and NGC 7582 (Prieto et al. 2010 and references therein). For NGC 1386, the X-ray luminosity has been derived from the 2-10 keV X-ray flux from Iyomoto et al. (1997) assuming a luminosity distance of 15.3 Mpc.
* for Circinus, NGC 1097 and NGC 7582, in addition to the AGN-associated warm gas, there are clumps of H_2 gas associated with star formation; † For NGC 1068 and NGC 1386, elliptical apertures of ellipticity 0.6 and 0.7 were used, respectively; †† The H_2 molecular gas properties of NGC 7582 come from SINFONI data.

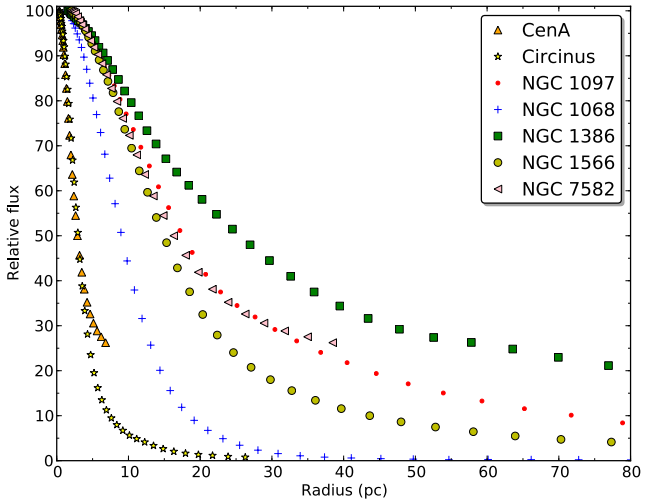

Figure 2. Distribution of the warm H_2 gas provided by the fit of circular isophotes (elliptical for NGC 1068 and NGC 1386) to the NaCo emission (SINFONI for NGC 7582). Fitting a Sérsic function indicates an exponential profile for all sources, with a mean HWHM of 27 pc.

of Circinus, additional clumpy H_2 warm gas emission is observed south and north of the nucleus at a 3σ level. The northern clumps seem to be associated with star formation, while the southern ones are most likely heated by the nuclear source (see Appendix A). Taking these clumps into account, we estimate for Circinus a total extent of the nuclear H_2 warm gas of 2 arcsec (38 pc) and an average extent of the nuclear H_2 warm gas emission for the whole sample of 127 pc. This total extent was defined as the maximum size of the 3σ distribution in our maps. The fit of a Sérsic function to the light profiles of the warm H_2 gas (Fig. 2) indicates exponential distributions (n∼1) for all sources and that the warm H_2 gas emission is concentrated at the centre with an average half width at half-maximum (HWHM) of 27 pc. This HWHM is in agreement with the average extent of the H_2 warm gas emission in Seyfert galaxies when traced by IFU observations (e.g. Hicks et al. 2009 find an average HWHM∼30 pc for a sample of Seyfert galaxies that includes Circinus, NGC 1068 and NGC 1097 observed by SINFONI with a FoV of up to 3.2 arcsec × 3.2 arcsec). When using a larger FoV (e.g. up to 8 arcsec × 8 arcsec; Mazzalay et al. 2013; Hicks et al. 2013), the molecular H_2 warm gas is observed to extend up to a few 100 pc (e.g. 144 pc for NGC 4536; Mazzalay et al. 2013; up to 250 pc for the five Seyfert galaxies of Hicks et al. 2013) similarly to what we find for our sample when observed by NaCo. Hicks et al. (2013) also study the extent and luminosity of a matched-sample of quiescent galaxies, finding that these present a flatter luminosity profile and lower H_2 luminosities within a radius of ∼100 pc than their sample of Seyferts. The sample of seven Seyfert galaxies we study in this paper has an average nuclear H_2 luminosity of 1.4×10^{39} erg s^{-1} (3.6×10^{5} L$_\odot$; see Table 2), which is one order of magnitude higher than that of the sample of quiescent galaxies of Hicks et al. (2013) and of the only non-AGN (NGC 3351) included in the sample of Mazzalay et al. (2013), and a more centrally concentrated nuclear H_2 distribution than that of the quiescent/non-AGN. These results are in agreement with those found by Hicks et al. (2013), suggesting that the nuclear H_2 molecular gas in the AGN constitutes a gas reservoir of material available for fuelling the central SMBH (see also Section 4.5).

4.2 NaCo versus SINFONI

The large FoV of the narrow-band NaCo imaging allows us to trace the distribution of the warm molecular H_2 gas beyond the instrument-limited small nuclear regions traced by IFU instruments as SINFONI. The different extent and morphology of the molecular H_2 warm gas traced by NaCo compared to that traced by a SINFONI FoV of up to ∼ 2 arcsec × 2 arcsec can be directly observed in Figs. 3–8 for CenA, Circinus, NGC 1097, NGC 1068, NGC 1386 and NGC 1566. In all these cases the H_2 warm gas in the NaCo maps extends beyond the SINFONI FoV, up to ∼ 6 – 8 arcsec (a few 100 pc) for most galaxies. For some sources like Circinus, the gas presents a complex morphology very distinct to the relatively symmetric distribution traced by SINFONI, while in others like NGC 1097 the extension of the H_2 emission seems to have a different orientation for NaCo and SINFONI. These morphological differences are not caused by

a higher SINFONI spatial resolution, as this is in many cases comparable or even lower than that of NaCo (e.g. for NGC 1097 the SINFONI spatial resolution is $FWHM_{SINFONI}$=0.25 arcsec, Davies et al. 2009, while $FWHM_{NaCo}$=0.14 arcsec, see Table 1; for CenA $FWHM_{SINFONI}$=0.12 arcsec, Neumayer et al. 2007, while $FWHM_{NaCo}$=0.12 arcsec; for Circinus $FWHM_{SINFONI}$=0.22 arcsec, Müller Sánchez et al. 2006, while $FWHM_{NaCo}$=0.16 arcsec). The differences between the NaCo and SINFONI H_2 intensity maps can be ascribed to the technique used to extract the H_2 line map from the SINFONI data cube: the continuum subtraction from the SINFONI data cube (e.g. in the case of NGC 1068; Müller Sánchez et al. 2009) relies on the equivalent width of the CO bands. Thus, the derived H_2 emission and morphology are quite uncertain in the nucleus, where the CO bands are almost diluted by the contribution of the non-stellar emission. This can seriously affect the morphology of the inner regions, as clearly evidenced for NGC 1068: a nuclear hole is observed in the warm H_2 emission-line map of Müller Sánchez et al. (2009) (see SINFONI map in Fig. 5), which is not present in the NaCo H_2 emission map. We note that such nuclear hole is not present either in the warm H_2 emission map of Barbosa et al. (2014), in agreement with the NaCo map presented in this work. Therefore, the NaCo image does recover more H_2 emission than the SINFONI maps shown in Fig. 5.

In order to check for consistency, we extract the H_2 1–0 S(1) 2.12 μm line flux within an aperture in the NaCo H_2 image equivalent to that of the SINFONI FoV (see Table 3). This is performed for those galaxies for which both NaCo and SINFONI molecular H_2 gas fluxes are available (CenA, Circinus, NGC 1097, NGC 1386, and NGC 1566). For NGC 1068 such a comparison is not viable due to the nuclear hole in the SINFONI H_2 emission-line map. Given the higher sensitivity of NaCo, the H_2 1–0 S(1) line fluxes measured with this instrument are expected to be higher than those obtained with SINFONI. This is indeed the case for Circinus, NGC 1097 and NGC 1386, for which the NaCo H_2 1–0 S(1) line flux is one to three orders of magnitudes larger than that from SINFONI. However, for CenA and NGC 1566 the NaCo H_2 1–0 S(1) line flux is one to two orders of magnitude smaller than the SINFONI flux. No polluting lines or features are observed in the region of the SINFONI spectrum close to the H_2 1–0 S(1) line, indicating that the H_2 1–0 S(1) line flux difference must be caused either by the flux calibration of the SINFONI data cubes or the continuum subtraction in the NaCo narrow-band filter. Calibration problems in the SINFONI data cube for the particular case of CenA could explain flux differences between NaCo and SINFONI of up to a factor 4, since the SINFONI observations were acquired under variable conditions (Burtscher, private communication). For instance, Israel et al. (1990) determined a well-calibrated H_2 1–0 S(1) flux in a 6 arcsec aperture of $(4.2 \pm 0.5) \times 10^{-14}$ erg cm^{-2} s^{-1}, which is of the same order as the NaCo flux.

Table 3. Comparison of NaCo and SINFONI fluxes

Object	Aperture [″]	H_2 1–0 S(1) flux NaCo [erg cm^{-2} s^{-1}]	H_2 1–0 S(1) flux SINFONI [erg cm^{-2} s^{-1}]
CenA	3×3	1.5×10^{-14}	3.4×10^{-13}
Circinus	0.8×0.8	1.2×10^{-14}	9.0×10^{-15} *
NGC 1097	4×4	5.9×10^{-14}	9.1×10^{-15}
NGC 1386	4×4	7.3×10^{-14}	2.2×10^{-14}
NGC 1566	3×3	7.7×10^{-14}	5.8×10^{-13}

* The SINFONI H_2 1–0 S(1) line flux of Circinus is taken from Müller Sánchez et al. (2006).

4.3 Comparison with dust and cold molecular gas

To characterize whether the molecular H_2 warm gas follows the dust and/or is coincident with regions of star formation, the H_2 warm gas contours are plotted on top of the dust maps of each galaxy and on top of the *K*-band or *I*-band maps for those galaxies with clumps of star formation. An individual description of each galaxy and of its H_2 and dust morphology is provided in the Appendix A. In CenA, NGC 1097, NGC 1566 and NGC 7582 the nuclear warm H_2 gas presents a diffuse, symmetrical morphology that does not correlate with that of the dust. The observed differences are not caused by a different FWHM between the dust maps and H_2 (NB2.12) images (see Table 1), but reflect a real different morphology. In Circinus (southern emission), NGC 1068 and NGC 1386 the morphology of the H_2 gas seems to reproduce that of the dust filaments close to the nucleus. However, the correspondence between the warm H_2 gas and the dust is not one to one. The lanes of warm H_2 gas observed in NGC 1068 and NGC 1386 are wider than the narrow dust filaments and more extended, filling gaps in the dust morphology. This is also observed in other Seyfert galaxies like NGC 7743 (Davies et al. 2014) and suggests that gas and dust trace *two different phases* at scales close to the nuclear region: once dust and gas approach the central few 100 pc, the gas is first warmed up by the nucleus (and/or in some cases jet shocks; see Section 4.4) and thus presents a wider and more extended morphology, while the dust remains a colder phase with a temperature well below 2000 K. This suggests that the dust morphology should resemble that of the cold molecular gas (e.g. CO at 10-40 K). The latter can be tested in those galaxies for which high angular resolution millimetre observations have been performed using ALMA (Cen A, Espada 2013; NGC 1068, García-Burillo et al. 2014; NGC 1097, Izumi et al. 2013; NGC 1566, Combes et al. 2014). In NGC 1566, a dual spiral structure of cold CO(3-2) gas emission is observed to emerge up to 300 pc from the nuclear region and to indeed coincide with the dust extinction (Fig. 8, bottom-left panel; see also Combes et al. 2014). Such a spiral structure is however not observed in our molecular H_2 warm gas emission map despite the large FoV of NaCo (Fig. 8, bottom right panel). A good correlation between the cold CO(3-2) gas emission and dust is also observed for the Seyfert 2 galaxy NGC 1433 (Combes et al. 2013) and for NGC 1068 (García-Burillo et al. 2014). The suggested *two phases of accretion* in which dust remains colder than the gas when approaching the nuclear (few 100 pc) scales is also clearly illustrated in CenA: a spatial anticorrelation is observed between the warm H_2 and cold CO(2-1) gas, with the H_2 filling the central ∼2 arcsec region devoid of cold gas (Fig. 3, bottom right panel), while the cold CO(2-1) gas seems to extend in the same direction as the dust filament that comes from a few tens of pc to the nucleus (Fig. 3, bottom-left panel). In the case of CenA the warm H_2 gas distribution presents a shell-like structure that extends along the direction of the radio jet (see Fig. 3, middle-left panel), where no cold CO(2-1) gas emission is observed (Fig. 3, bottom panels). This warm H_2 gas morphology and the lack of cold gas emission in that direction are thus most likely caused by jet bow shocks (see Section 4.4).

While the cold molecular gas distribution resembles the morphology of the dust but not that of the warm molecular gas, as predicted by the *two phases of accretion* scenario and observed in all the target sources for which ALMA observations are available,

the warm (1000-3000 K) and cold (10-40 K) molecular gas are part of the same dynamical structure and should thus show similar morphologies (or not be completely spatially decoupled) at 'mixed' or 'intermediate' temperatures of e.g. 40-500 K. A good illustration of this is observed in NGC 1068 and NGC 1097: the morphology of the warm H_2 gas closely resembles that of the slightly warm molecular gas (T >40 K) such as CO(6-5) or HCN, among others, as shown in the ALMA images of NGC 1068 (Fig. 5, bottom right panel) and NGC 1097 (Fig. 6, bottom-left panel; see also Izumi et al. 2013, Martín et al. 2015), while, as expected from the *two phases of accretion* scenario, the warm H_2 gas appears disconnected from the cold dust (e.g. Fig. 6, middle-left panel).

4.4 Source of the warm H_2 molecular gas emission

To explain the excitation of the warm H_2 gas, we look for evidence of spatially associated star formation, shocks produced by jet interaction or thermal heating by X-rays. Clumps of warm molecular H_2 gas emission coincident with regions of star formation in the *HST I*-band, NaCo/*K*-band or ESO/VISIR mid-IR bands are observed in the northern spiral arm of Circinus (Fig. 4, see Appendix A), the starburst ring of NGC 1097 (Fig. 6) and NGC 7582 (Fig. 9). In these regions, star formation is the heating mechanism that excites the H_2 molecules. Apart from these clumps, no warm H_2 gas emission is observed beyond scales of a few 100 pc despite the large FoV (∼30 arcsec) of the H_2 intensity maps. We thus conclude that the H_2 maps obtained with NaCo show the majority of the warm H_2 molecular gas present in the studied galaxies.

No clumps of star formation are observed in the nuclear region of any of the sources (except for the northern spiral arm of Circinus mentioned above), indicating that the central warm H_2 gas is heated by the AGN. In nuclear regions, the H_2 molecules are found to be typically excited by thermal processes (e.g. Rodríguez-Ardila et al. 2004; Mazzalay et al. 2013; Combes et al. 2014) due to either shocks (Hollenbach & McKee 1989) or X-ray illumination (Maloney et al. 1996). Most of the galaxies studied here were analysed in Reunanen et al. (2003) using long-slit near-IR data. On the basis of the H_2 2-1S(1)/1-0S(1) ratio, thermal excitation was favoured as the dominant mechanism for the nuclear H_2 observed in their sample of 14 Seyfert galaxies. In the present study, where we trace the whole distribution of warm H_2 within the central kpc region, we can state that no young star formation is seen associated with the central but spatially extended H_2 emission in any of the galaxies: no evidence for it is seen at the centre in our high angular resolution *K*-band images. UV photons are thus not the cause of the source of H_2 excitation, in agreement with the Reunanen et al. (2003) conclusion.

We find, however, a fair spatial correlation between the H_2 and the X-ray morphology, which is particularly evident in those cases where the X-ray and H_2 emission is seen spatially resolved at the centre: for NGC 1068 and NGC 1386, the nuclear X-ray emission presents an extension and morphology that resembles that of the warm H_2 molecular gas (middle-right panel in Fig. 5, for NGC 1068, and bottom-right panel Fig. 7, for NGC 1386) and is coincident with the extent and morphology of the narrow-line region traced by the [OIII] ionized gas (Capetti et al. 1997; Bianchi et al. 2006; Wang et al. 2012), suggesting that both the diffuse X-ray and the [O III] emission are produced by the same gas photoionized by the nuclear continuum (e.g. Iwasawa et al. 2003; Wang et al. 2012). The extension of the nuclear 0.3-10 keV band X-ray emission is also comparable to the nuclear warm H_2 gas distribution in NGC 1097, NGC 7582 and Circinus (Figs. 4, 6, 9, bottom right panel) indicating that the nuclear warm H_2 molecular gas is most likely excited by the X-ray emission of the photoionized gas, as it was also suggested for e.g. the Seyfert galaxies NGC 4151, NGC 5548 and NGC 3227 (Rodríguez-Ardila et al. 2004; Storchi-Bergmann et al. 2009). The nuclear X-ray emission traced by the *Chandra* X-ray satellite for CenA (Evans & Koratkar 2004) is observed to cover an area larger than the extent of the nuclear warm H_2 molecular gas. For NGC 1566, the X-ray emission is unresolved (Fabbiano et al. 1992) and does not allow a direct morphological comparison with the warm H_2 gas distribution.

Table 4. Predicted H_2 2.12μm fluxes from the X-ray models of Maloney et al. (1996) for a gas density of 10^5 cm^{-3}.

Object	$N_{\rm H_{att}}$ [10^{22} cm^{-2}]	H_2 1–0 S(1) flux Predicted [erg cm^{-2} s^{-1}]	Observed [erg cm^{-2} s^{-1}]	Predicted if f=10% [erg cm^{-2} s^{-1}]
CenA	2.4	1.2×10^{-14}	1.6×10^{-14}	1.2×10^{-13}
Circinus	1.3	3.9×10^{-15}	1.9×10^{-14}	3.9×10^{-14}
NGC 1068	0.4	4.5×10^{-15}	7.1×10^{-14}	4.5×10^{-14}
NGC 1097	0.04	6.0×10^{-15}	5.4×10^{-14}	6.0×10^{-14}
NGC 1386	0.5	1.4×10^{-16}	6.6×10^{-14}	1.4×10^{-15}
NGC 1566	0.6	9.1×10^{-15}	8.9×10^{-14}	9.1×10^{-14}
NGC 7582	0.9	2.1×10^{-16}	3.4×10^{-15}	2.1×10^{-15}

* Predicted H_2 2.12μm fluxes assuming a conservative filling factor of 10%.

Hard X-ray photons can easily penetrate the molecular clouds before being absorbed and heat the medium to excite the 2μm vibration-rotation lines of H_2. We test this possibility from the energy balance point of view by comparing the observed H_2 fluxes with those predicted in the models of Maloney et al. (1996). These models investigate the effects of X-ray irradiation on molecular gas and predict H_2 fluxes for a wide range of X-ray impinging luminosities and densities. We follow a similar approach as in Rodríguez-Ardila et al. (2004). Accordingly, we determine the effective ionization parameter, defined in Maloney et al. (1996) as follows:

$$\zeta \simeq 100 \frac{L_{\rm X}}{n_{\rm e} d^2 N_{\rm H_{att}}^{0.9}} \quad (1)$$

where $L_{\rm X}$ is the hard X-ray luminosity in units of 10^{44} erg s^{-1}, $n_{\rm e}$ the total gas density in units of 10^5 cm^{-3}, d the distance in pc of the emitting gas to the AGN, and $N_{\rm H_{att}}$ the attenuating column density to the X-rays in units of 10^{22} cm^{-2}, and we use Fig. 6 in Maloney et al. (1996) assuming $n_{\rm e}$=10^5 cm^{-3}. The X-ray nuclear luminosities are taken for most sources from Prieto et al. (2010), who compile fluxes at energies above 20 keV. These reflect the truly X-ray emerging flux from the nucleus, particularly for the Compton thick sources in the sample. For NGC 1386, we use the 2–10 keV X-ray flux from Iyomoto et al. (1997). The average X-ray luminosity of the sample is ∼ 10^{42} erg s^{-1} (see Table 2). The attenuating $N_{\rm H}$ correspond to the $A_{\rm v}$ extinction values derived by Reunanen et al. (2002) and Prieto et al. (2005, 2010, 2014) for the central few 100 pc in these galaxies, which is within the radius the H_2 emission is observed. We used the conversion factor $N_{\rm H}$= (1.79 ± 0.03) × 10^{21} cm^{-2} $A_{\rm v}$ (Predehl & Schmitt 1995). The values of $N_{\rm H_{att}}$ obtained are typically in the range 10^{21}–10^{22} cm^{-2} (see Table 4). The radius of the nuclear extended H_2 emission is taken from Table 2.

The predicted H_2 flux apparently agrees well with the one

measured only for CenA. However, considering the uncertainties in the determination of the ionization parameter, which could be up to an order of magnitude higher if allowed for lower $N_{\rm H_{att}}$, the predicted H_2 fluxes are within the range of observed values also for Circinus, NGC 1097 and NGC 1566 (see Table 4). In the remaining three, the prediction is an order of magnitude less, even if $N_{\rm H_{att}}$ is allowed to get reduced by an order of magnitude –this is because the dependence of the H_2 flux on ζ is weak for the range of ζ derived for these sources. Also much lower $N_{\rm H}$ would expose easily the core of the H_2 molecular cloud to the X-rays and would become fully ionized. The underpredicted H_2 fluxes are thus surprising given the spatial association between the H_2 and the X-rays. Yet, we know that the interstellar medium in galaxies is very clumpy, with molecular gas clouds having average sizes in the 10-100 pc range, and filling factors of a few percent are estimated for the cold dense phase (McKee & Ostriker 1977). A way to reconcile the above results is thus to assume a filling factor in the molecular gas region so that the observed emission arises from the most clumpy regions inside the molecular gas region that have higher densities; this would also explain the relatively large radii at which H_2 emission is detected. Our knowledge of the filling factor of molecular clouds in the environment of AGN is poor, yet assuming filling factors (f) in the range of 1% to 10%, in line with the values adopted by McKee & Ostriker (1977) in their three-component medium of the interstellar medium, would bring the results to agreement (Table 4, last column). An exception is NGC 1386, where the H_2 emission is the largest among the objects in the sample. This source has a jet (Nagar & Wilson 1999) of size$\sim$100 pc and power 1.2×10^{42} erg s^{-1} (Mezcua & Prieto 2014) pointing to the south direction and coinciding in location with the southern extension in H_2, thus shocks induced by the jet might in this case be the local source of H_2 excitation.

Shock excitation of the H_2 molecule caused by jet interactions could also take place in CenA and NGC 1097, who have a radio jet of total size $\sim$2 kpc and $\sim$0.1 kpc, respectively, and values of jet power (6×10^{42} erg s^{-1} for CenA and 1.5×10^{41} erg s^{-1} for NGC 1097; e.g. Mezcua & Prieto 2014 and references therein) several orders of magnitude larger than the H_2 luminosity. For CenA, this is supported by the well-defined shell-like structure of the warm H_2 molecular gas emission, which extends perpendicular to the direction of the radio jet, and by the finding of a large H_2/PAH (polycyclic aromatic hydrocarbon) ratio, which rules out UV excitation in photodissociation regions as the source of the H_2 line excitation (Ogle et al. 2010). Therefore, although CenA is the only source in the sample that is comfortably explained by thermal excitation by X-rays (see Table 4, column 4), the bow shock morphology of the H_2 gas emission and apparent fair alignment between the H_2 gas and the jet direction qualitatively points to shocks induced by the jets as a plausible additional mechanism for exciting the H_2 gas. In NGC 1068, a recent episode of star formation ($\sim$30 Myr ago; Storchi-Bergmann et al. 2012) was found to occur in the ring-like structure of warm H_2 gas located at $\sim$100 pc from the nucleus. According to simulations, the formation of such rings and star formation at radii of $\sim$ 100 pc could result from the shock waves created by a young radio jet (Gaibler et al. 2012). The excitation of warm H_2 molecular gas ring-like structure in NGC 1068 could thus be also explained by a shock jet interaction (see Fig. 5, middle-left panel). In this case, the off-centred nuclear position of the ring could be explained by inhomogeneities in the gas that surrounds the nucleus (Barbosa et al. 2014).

The large extent of the nuclear warm H_2 gas, up to scales of a few 100 pc, can be thus explained for all the targets by thermal processes, in agreement with previous studies (e.g. Rodríguez-Ardila et al. 2004; Mazzalay et al. 2013; Combes et al. 2014). Given the similar symmetrical morphology between the nuclear X-ray and warm H_2 molecular gas emission, X-ray heating is the most likely excitation source of the nuclear warm H_2 gas for most sources, possibly also combined with shocks from radio jets for CenA, NGC 1097 and NGC 1068.

Finally, we note that the nuclear X-ray luminosity of the target sources is one to four orders of magnitude larger than the nuclear H_2 luminosity (see Table 2), indicating that a small fraction of X-ray photons penetrating and heating the central H_2 molecular gas cloud is enough to excite the H_2 gas. The X-ray luminosities of the AGN studied here are also two to four orders of magnitude higher than those of the quiescent galaxies of Hicks et al. (2013) (see also Mazzalay et al. 2013), which show not so centrally concentrated nuclear warm H_2 gas distributions and lower H_2 luminosities than the AGN, thus reinforcing the AGN X-ray emission as the dominant excitation mechanism of the warm H_2 molecular gas.

4.5 Molecular gas mass and density

The large FoV of the NaCo observations reveals the extent and morphology of all the warm molecular H_2 gas present in the studied galaxies at scales of a few 100 pc. Following Reunanen et al. (2002), the mass of this warm H_2 gas ($M_{\rm warm}$) is quantified using the flux extracted from the H_2 intensity maps and assuming a gas temperature of 2000 K, the H_2 1–0S(1) transition probability $A_{S(1)}$ = 3.47 $\times$ 10^{-7} s^{-1} (Turner et al. 1977) and the population fraction of the (ν, J) = (1,3) level $f_{(1,3)}$ = 0.0122 (Scoville et al. 1982) as:

$$M_{\rm warm} = 5.0875\times10^{13}\left(\frac{D_L}{\rm Mpc}\right)^2\frac{F_{1-0S(1)}}{\rm erg\,s^1cm^{-2}}10^{0.4277A_{2.2}} \quad (2)$$

where $A_{2.2}$ is the extinction at 2.2 μm (Scoville et al. 1982). The H_2 flux was extracted in a nuclear circular aperture for CenA, Circinus, NGC 1068, NGC 1097, NGC 1566 and NGC 7582, and an elliptical aperture for NGC 1068 and NGC 1386 with a size corresponding to the extent of the warm H_2 gas emission given by the isophote fitting (Table 2). The values of $A_{2.2}$, derived from regions surrounding the nucleus, are taken from Reunanen et al. (2002) for CenA and NGC 1566, Prieto et al. (2005) for NGC 1097, Prieto et al. (2010) for Circinus and NGC 1068 and Prieto et al. (2014) for NGC 1386 and NGC 7582, and range between $A_{2.2}$ = 0.2 and 1.6 for all sources. The masses of the nuclear warm H_2 gas are reported in Table 2 and range between 40 M$_\odot$ (for Circinus) and 3000 M$_\odot$ (for NGC 1566).

In Section 4.1 we found that the nuclear H_2 luminosity of the sample is on average 10 times higher than that of the quiescent sources from Hicks et al. (2013) and Mazzalay et al. (2013). The mass of the AGN molecular gas reservoir is thus $\sim$ 10 times higher for the Seyfert galaxies studied here than for the quiescent galaxies (as found by Hicks et al. 2013). This suggests that either these AGN have more material available for accretion on to the central SMBH than the non-AGN galaxies, which could also explain the higher X-ray luminosities of the Seyfert galaxies, or that the gas is more effectively heated by the AGN in the Seyfert galaxies, so that in these we see the H_2 emission while in the normal galaxies the H_2 gas remains invisible.

The total content of molecular cold gas can be estimated using a correlation between H_2 2.12 μm luminosity and cold gas mass derived from CO observations (e.g. Dale et al. 2005; Müller Sánchez et al. 2006; Mazzalay et al. 2013). This allows us to obtain an estimate of the amount of cold gas present in the nuclear

regions and thus available for accretion on to the AGN. Using the $M_{\rm cold}$–$L_{\rm H2}$ relation of Mazzalay et al. (2013), equation 4, we obtain that the cold H_2 gas mass ranges between $7 \times 10^6\,{\rm M}_\odot$ (for CenA) and $1 \times 10^9\,{\rm M}_\odot$ (for NGC 1566; see Table 2). The value of $M_{\rm cold}$ obtained for NGC 1566 is in agreement with the total molecular mass of $1.3 \times 10^9\,{\rm M}_\odot$ obtained from CO Swedish-ESO Submillimetre Telescope (SEST) observations but one order of magnitude lower than the $M_{\rm cold}$ obtained from smaller FoV CO observations (e.g. 18 arcsec with ALMA; see Combes et al. 2014 for a discussion), which indicates that NaCo recovers the total content of molecular gas for NGC 1566. For CenA, Circinus and NGC 1068, the estimated values of $M_{\rm cold}$ are one order of magnitude lower than those obtained from CO observations (Curran et al. 1998; Schinnerer et al. 2000; Espada et al. 2009), which can be mainly attributed to the larger FoV of the CO observations. We note though that better agreement would not be achieved even if we considered a larger aperture for the warm H_2 gas, as (except for the clumps in the spiral arm of NGC 1097) most of the detected warm H_2 gas is concentrated in the nuclear regions and no emission is observed further out despite the large FoV of NaCo.

Given that the morphology of the nuclear warm H_2 molecular gas appears diffuse and symmetrical in most sources, we can estimate its density assuming a spherical volume with a gas mass fraction (or gas-to-mass ratio) $f_{\rm g}$=1% for NGC 1097 and $f_{\rm g}$=10% for the rest of the sources (following Hicks et al. 2009). This $f_{\rm g}$ represents the fraction of the volume occupied by a certain gas phase and should not be confused with the filling factor (f) introduced in Section 4.4[8]. The volume is derived using the same radius as that considered when calculating the nuclear H_2 gas masses. We obtain cold gas densities ranging $N_{\rm cold}$= 6×10^3 – 1×10^5 cm^{-3}, which is consistent with the $N_{\rm H_2}$= 10^4–10^5 cm^{-3} typically derived from CO observations (e.g. Mauersberger & Henkel 1989; Bayet et al. 2009).

5 CONCLUSIONS

In this paper we have presented the morphology and properties of the warm molecular H_2 gas of a sample of seven nearby Seyfert galaxies observed with VLT AO and narrow-band imaging with NaCo. Dust colour maps of these galaxies are also constructed using the ratio between broad-band *K*-band images and *V*- and *I*-band *HST* images. The large FoV of the observations has allowed us to trace the distribution of the warm H_2 gas and dust up to scales of a few 100 pc with a resolution < 0.5 arcsec.

For all galaxies, the warm H_2 gas is concentrated in the nuclear regions (with an HWHM of 27 pc) and does not extend beyond $\sim$ 300 pc from the nucleus. The warm H_2 gas is thus visible when the gas is close enough to the heating source (the nucleus, where the peak of H_2 emission is observed) and the H_2 molecules are excited enough to produce ro-vibrational emission lines. Further out, the H_2 gas is not warm enough and only the cold gas is visible through e.g. CO observations. In NGC 1097, Circinus and NGC 7582 some clumps or lanes of H_2 emission are in addition observed to coincide with regions of star formation.

The excitation mechanism for all the target sources is found to be thermal. The cospatial location of H_2 and X-rays, also coinciding on physical extension in those cases where spatial resolution allows for size measurements, is a strong indication for nuclear X-rays being the major source of excitation of H_2. We conclude that irradiation by X-rays is the predominant source of excitation for most sources under reasonable assumptions of the H_2 clouds volume filling factor (of 10%).

In NGC 1068, NGC 1386, NGC 1566 and Circinus, the morphology of the warm H_2 gas traced either by NaCo or IFU observations resembles within a few tens of pc that of the filamentary dust lanes that extend from the central parsecs to $\sim$ 1 kpc scale. These dust filaments are potential fuelling channels that transport the gas to the nuclear region. This suggests that the nuclear warm H_2 gas of these galaxies comes from outer (kpc-scale) regions following these same channels of inflow and warms up as it approaches the nucleus. The observed lanes of warm H_2 gas are however much wider and extended than the filaments of dust, which suggests that gas and dust trace *two different states of accretion with different temperatures*. In such scenario the nuclear dust morphology at scales of a few 100 pc should resemble that of the cold (10-40 K) molecular gas, as we observe for CenA and NGC 1566 by ALMA CO observations, while the inner warm (1000-3000 K) H_2 gas presents a wider morphology that should resemble that of the slightly warmed gas (40-500 K), as indicated by warmer molecular tracers (e.g. CO(6-5), HCN) observed in NGC 1068 and NGC 1097 with ALMA.

6 ACKNOWLEDGEMENTS

The authors thank F. Israel for comments on the manuscript. The authors are indebted to F. Müller-Sánchez for providing the SINFONI H_2 gas emission map of NGC 1068, O. González-Martín for the *Chandra* data, J. Wang for the *Chandra* image of NGC 1068, L. Burtscher for the SINFONI data cubes, F. Combes for the ALMA image of NGC 1566, D. Espada for the ALMA image of CenA, and S. García Burillo for the ALMA image of NGC 1068. MM acknowledges financial support from AYA2011-25527 and NASA *Chandra* grant G05-16099X. The research leading to the results has received funding from the European Community's Seventh Framework Programme under grant agreement 312430. Research by JAFO was supported by Canary Islands CIE: Tricontinental Atlantic Campus. This research is based on ESO VLT programmes P71.B-0632A, 74.B-0722B and 86.B-0484. The research has made use of the NASA/IPAC Extragalactic Database (NED) which is operated by the Jet Propulsion Laboratory, California Institute of Technology, under contract with the National Aeronautics and Space Administration.

REFERENCES

Alloin D., Pelat D., Phillips M., Whittle M., 1985, ApJ, 288, 205
Barbosa F. K. B., Storchi-Bergmann T., McGregor P., Vale T. B., Rogemar Riffel A., 2014, MNRAS, 445, 2353
Bayet E., Aladro R., Martín S., Viti S., Martín-Pintado J., 2009, ApJ, 707, 126
Bianchi S., Guainazzi M., Chiaberge M., 2006, A&A, 448, 499
Bicknell G. V., Sutherland R. S., Neumayer N., 2013, ApJ, 766, 36
Bourne M. A., Nayakshin S., Hobbs A., 2014, MNRAS, 441, 3055

[8] Hicks et al. (2009) assumed a uniform gas distribution in their work (this is, a filling factor of 100%) though the authors conclude that the gas must be clumpy. This implies a filling factor f <1, in line with the hypothesis made in Section 4.4 of assuming a filling factor for the H_2 molecular gas.

Capetti A., Macchetto F. D., Lattanzi M. G., 1997, ApJ, 476, L67
Clarke D. A., Burns J. O., Norman M. L., 1992, ApJ, 395, 444
Combes F., 2006, Formation and Evolution of Supermassive Black Holes. Springer, p. 159
Combes F. et al., 2013, A&A, 558, A124
Combes F. et al., 2014, A&A, 565, A97
Curran S. J., Johansson L. E. B., Rydbeck G., Booth R. S., 1998, A&A, 338, 863
Dale D. A., Sheth K., Helou G., Regan M. W., Hüttemeister S., 2005, AJ, 129, 2197
Davies R. I. et al., 2014, ApJ, 792, 101
Davies R. I., Maciejewski W., Hicks E. K. S., Tacconi L. J., Genzel R., Engel H., 2009, ApJ, 702, 114
Devillard N., 1999, in Mehringer D. M., Plante R. L., Roberts D. A., eds, Astronomical Society of the Pacific Conference Series Vol. 172, Astronomical Data Analysis Software and Systems VIII. p. 333
Di Matteo P., Bournaud F., Martig M., Combes F., Melchior A.-L., Semelin B., 2008, A&A, 492, 31
Englmaier P., Shlosman I., 2000, ApJ, 528, 677
Espada D., 2013, in Kawabe R., Kuno N., Yamamoto S., eds, Astronomical Society of the Pacific Conference Series Vol. 476, New Trends in Radio Astronomy in the ALMA Era: The 30th Anniversary of Nobeyama Radio Observatory. p. 69
Espada D. et al., 2009, ApJ, 695, 116
Evans I. N., Koratkar A. P., 2004, ApJ, 617, 209
Fabbiano G., Kim D.-W., Trinchieri G., 1992, ApJS, 80, 531
Fernández-Ontiveros J. A., Prieto M. A., Acosta-Pulido J. A., Montes M., 2012, Journal of Physics Conference Series, 372, 012006
Ferruit P., Wilson A. S., Mulchaey J., 2000, ApJS, 128, 139
Freeman K. C., Karlsson B., Lynga G., Burrell J. F., van Woerden H., Goss W. M., Mebold U., 1977, A&A, 55, 445
Gaibler V., Khochfar S., Krause M., Silk J., 2012, MNRAS, 425, 438
Galliano E., Alloin D., 2002, A&A, 393, 43
Gallimore J. F., Baum S. A., O'Dea C. P., Pedlar A., 1996, ApJ, 458, 136
García-Burillo S. et al., 2014, A&A, 567, A125
García-Burillo S. et al., 2009, A&A, 496, 85
Gaspari M., Ruszkowski M., Oh S. P., 2013, MNRAS, 432, 3401
Harris G. L. H., Rejkuba M., Harris W. E., 2010, PASA, 27, 457
Hicks E. K. S., Davies R. I., Maciejewski W., Emsellem E., Malkan M. A., Dumas G., Müller-Sánchez F., Rivers A., 2013, ApJ, 768, 107
Hicks E. K. S., Davies R. I., Malkan M. A., Genzel R., Tacconi L. J., Müller Sánchez F., Sternberg A., 2009, ApJ, 696, 448
Hlavacek-Larrondo J. et al., 2013, ApJ, 777, 163
Hollenbach D., McKee C. F., 1989, ApJ, 342, 306
Hopkins P. F., Hernquist L., Cox T. J., Di Matteo T., Robertson B., Springel V., 2006, ApJS, 163, 1
Hunt L. K., Malkan M. A., 2004, ApJ, 616, 707
Israel F. P., van Dishoeck E. F., Baas F., Koornneef J., Black J. H., de Graauw T., 1990, A&A, 227, 342
Iwasawa K., Wilson A. S., Fabian A. C., Young A. J., 2003, MNRAS, 345, 369
Iyomoto N., Makishima K., Fukazawa Y., Tashiro M., Ishisaki Y., 1997, PASJ, 49, 425
Izumi T. et al., 2013, PASJ, 65, 100
Jensen J. B., Tonry J. L., Barris B. J., Thompson R. I., Liu M. C., Rieke M. J., Ajhar E. A., Blakeslee J. P., 2003, ApJ, 583, 712
Jogee S., 2006, in Alloin D., ed., Lecture Notes in Physics, Berlin Springer Verlag Vol. 693, Physics of Active Galactic Nuclei at all Scales. p. 143
Koekemoer A. M., Fruchter A. S., Hook R. N., Hack W., 2003, in Arribas S., Koekemoer A., Whitmore B., eds, HST Calibration Workshop : Hubble after the Installation of the ACS and the NICMOS Cooling System. p. 337
Kormendy J., Ho L. C., 2013, ARA&A, 51, 511
Krips M. et al., 2011, ApJ, 736, 37
Maciejewski W., 2004, MNRAS, 354, 883
Malkan M. A., Gorjian V., Tam R., 1998, ApJS, 117, 25
Maloney P. R., Hollenbach D. J., Tielens A. G. G. M., 1996, ApJ, 466, 561
Marco O., Alloin D., Beuzit J. L., 1997, A&A, 320, 399
Marconi A., Moorwood A. F. M., Salvati M., Oliva E., 1994, A&A, 291, 18
Martín S. et al., 2015, A&A, 573, A116
Martini P., Regan M. W., Mulchaey J. S., Pogge R. W., 2003, ApJ, 589, 774
Mauersberger R., Henkel C., 1989, A&A, 223, 79
Mazzalay X. et al., 2013, MNRAS, 428, 2389
McKee C. F., Ostriker J. P., 1977, ApJ, 218, 148
Mezcua M., Prieto M. A., 2014, ApJ, 787, 62
Morganti R., Tsvetanov Z. I., Gallimore J., Allen M. G., 1999, A&AS, 137, 457
Müller Sánchez F., Davies R. I., Eisenhauer F., Tacconi L. J., Genzel R., Sternberg A., 2006, A&A, 454, 481
Müller Sánchez F., Davies R. I., Genzel R., Tacconi L. J., Eisenhauer F., Hicks E. K. S., Friedrich S., Sternberg A., 2009, ApJ, 691, 749
Nagar N. M., Wilson A. S., 1999, ApJ, 516, 97
Neumayer N., Cappellari M., Reunanen J., Rix H.-W., van der Werf P. P., de Zeeuw P. T., Davies R. I., 2007, ApJ, 671, 1329
Ogle P., Boulanger F., Guillard P., Evans D. A., Antonucci R., Appleton P. N., Nesvadba N., Leipski C., 2010, ApJ, 724, 1193
Orienti M., Prieto M. A., 2010, MNRAS, 401, 2599
Predehl P., Schmitt J. H. M. M., 1995, A&A, 293, 889
Prieto M. A., Maciejewski W., Reunanen J., 2005, AJ, 130, 1472
Prieto M. A., Marco O., Gallimore J., 2005, MNRAS, 364, L28
Prieto M. A. et al., 2004, ApJ, 614, 135
Prieto M. A., Mezcua M., Fernández-Ontiveros J. A., Schartmann M., 2014, MNRAS, 442, 2145
Prieto M. A., Reunanen J., Kotilainen J. K., 2002, ApJ, 571, L7
Prieto M. A., Reunanen J., Tristram K. R. W., Neumayer N., Fernandez-Ontiveros J. A., Orienti M., Meisenheimer K., 2010, MNRAS, 402, 724
Reunanen J., Kotilainen J. K., Prieto M. A., 2002, MNRAS, 331, 154
Reunanen J., Kotilainen J. K., Prieto M. A., 2003, MNRAS, 343, 192
Reunanen J., Prieto M. A., Siebenmorgen R., 2010, MNRAS, 402, 879
Rodríguez-Ardila A., Pastoriza M. G., Viegas S., Sigut T. A. A., Pradhan A. K., 2004, A&A, 425, 457
Rousset G. et al., 2003, in Wizinowich P. L., Bonaccini D., eds, Society of Photo-Optical Instrumentation Engineers (SPIE) Conference Series Vol. 4839, Society of Photo-Optical Instrumentation Engineers (SPIE) Conference Series. pp 140–149
Schinnerer E., Eckart A., Tacconi L. J., Genzel R., Downes D., 2000, ApJ, 533, 850
Schmitt H. R., Kinney A. L., 1996, ApJ, 463, 498

Scoville N. Z., Hall D. N. B., Ridgway S. T., Kleinmann S. G., 1982, ApJ, 253, 136
Sersic J. L., 1968, Atlas de galaxias australes. (Cordoba: Observatorio Astronomico)
Shlosman I., Frank J., Begelman M. C., 1989, Nature, 338, 45
Steinborn L. K., Dolag K., Hirschmann M., Prieto M. A., Remus R.-S., 2015, MNRAS, 448, 1504
Storchi-Bergmann T., Dors Jr. O. L., Riffel R. A., Fathi K., Axon D. J., Robinson A., Marconi A., Östlin G., 2007, ApJ, 670, 959
Storchi-Bergmann T., McGregor P. J., Riffel R. A., Simões Lopes R., Beck T., Dopita M., 2009, MNRAS, 394, 1148
Storchi-Bergmann T., Riffel R. A., Riffel R., Diniz M. R., Borges Vale T., McGregor P. J., 2012, ApJ, 755, 87
Terry J. N., Paturel G., Ekholm T., 2002, A&A, 393, 57
Tomono D., Terada H., Kobayashi N., 2006, ApJ, 646, 774
Tristram K. R. W., Burtscher L., Jaffe W., Meisenheimer K., Hönig S. F., Kishimoto M., Schartmann M., Weigelt G., 2014, A&A, 563, A82
Tully R. B., Rizzi L., Shaya E. J., Courtois H. M., Makarov D. I., Jacobs B. A., 2009, AJ, 138, 323
Turner J., Kirby-Docken K., Dalgarno A., 1977, ApJS, 35, 281
Ulvestad J. S., Wilson A. S., 1984, ApJ, 285, 439
van Dokkum P. G., 2001, PASP, 113, 1420
Wada K., 2012, ApJ, 758, 66
Wang J., Fabbiano G., Karovska M., Elvis M., Risaliti G., 2012, ApJ, 756, 180
Wold M., Galliano E., 2006, MNRAS, 369, L47

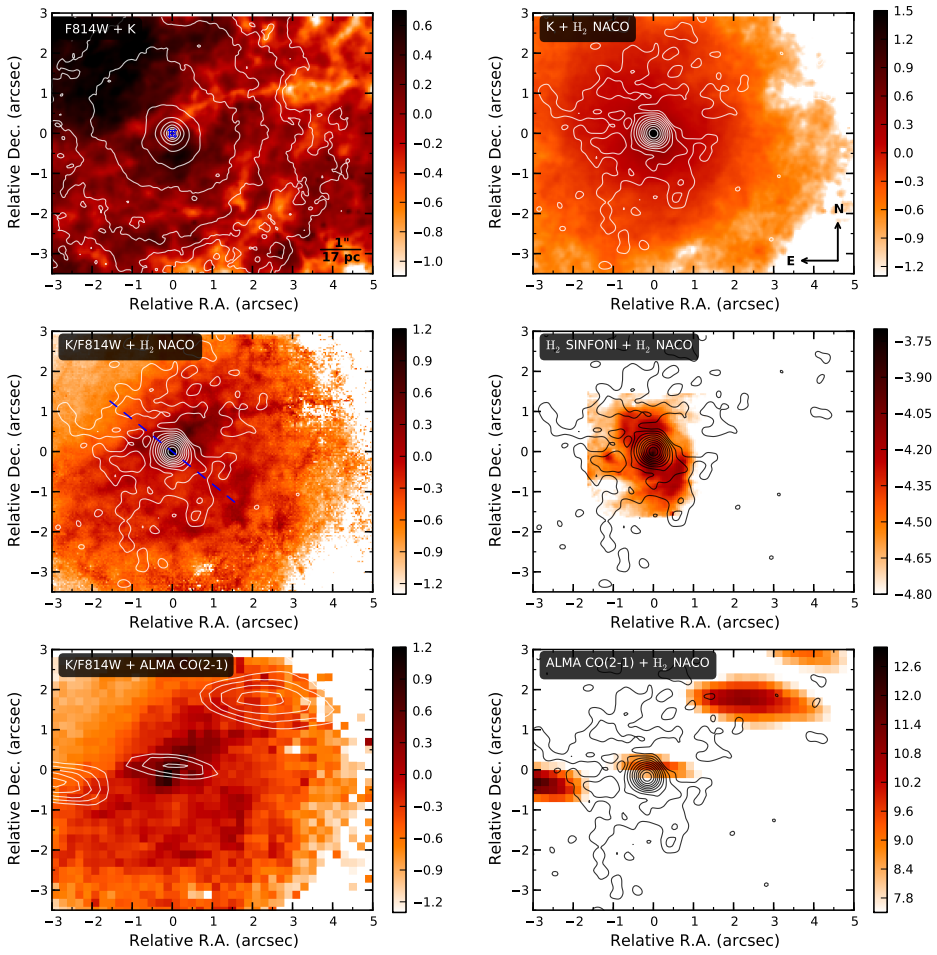

Figure 3. CenA. **Top left**: *HST/F814W* image with NaCo/*K*-band continuum contours in white. The position of the nucleus and its error is marked with a cross. **Top right:** NaCo/*K*-band image. The contours of the warm H_2 molecular gas obtained from NaCo are shown in white. They start at three times the background noise level and increase in factors of 2. **Middle left:** *K/F814W* ratio or dust map. The contours of the warm H_2 molecular gas obtained from NaCo are shown in white. The orientation of the radio jet (e.g. Clarke et al. 1992) is indicated with a dashed blue line. **Middle right:** Intensity map of the warm H_2 molecular gas obtained from IFU SINFONI. The contours of the warm H_2 molecular gas obtained from NaCo are shown in black. **Bottom left:** *K/F814W* ratio or dust map. The contours of the cold CO(2-1) molecular gas obtained from ALMA (Espada 2013) are shown in white. Contours start at three times the rms noise of 2.5 mJy beam^{-1} (Espada 2013). **Bottom right:** ALMA CO(2-1) integrated intensity map (from Espada 2013). The contours of the warm H_2 molecular gas obtained from NaCo are shown in black. The colour scale is linear and starts at three times the rms noise of 2.5 mJy beam^{-1}. The colour palettes in the other panels are in arbitrary units. The FoV for all panels is 8 arcsec × 6 arcsec. North is up and east is to the left.

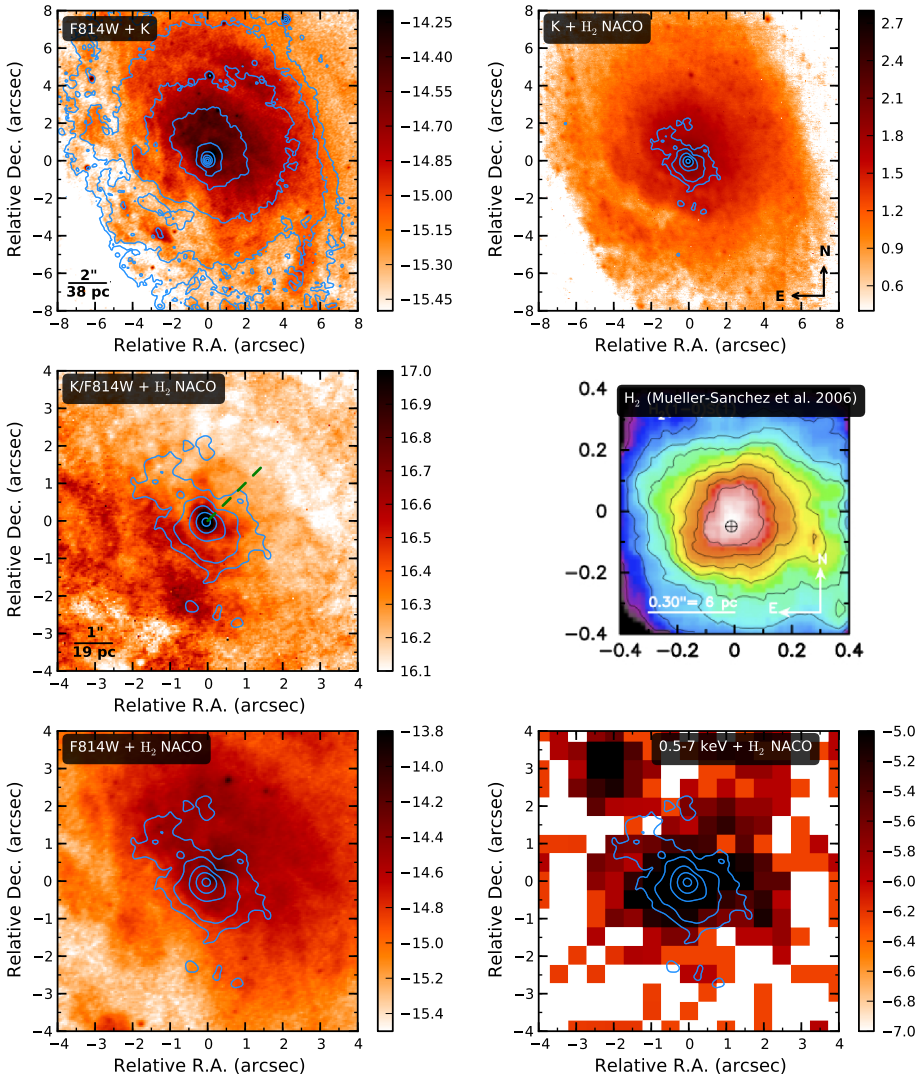

Figure 4. Circinus. **Top left**: *HST/F814W* image with NaCo/*K*-band continuum contours in blue. The FoV is 16 arcsec × 16 arcsec. **Top right:** NaCo/*K*-band image with the same FoV as the previous panel. The contours of the warm H_2 molecular gas obtained from NaCo are shown in blue. They start at three times the background noise level and increase in factors of 3. **Middle left:** *K/F814W* ratio or dust map with a FoV of 8 arcsec × 8 arcsec. The contours of the warm H_2 molecular gas obtained from NaCo are shown in blue. The orientation of the narrow line region (e.g. Marconi et al. 1994) is indicated with a dashed green line. **Middle right:** Intensity map of the H_2 molecular gas obtained from IFU SINFONI (from Müller Sánchez et al. 2006). **Bottom left:** *HST/F814W* image with a FoV of 8 arcsec × 8 arcsec. The contours of the warm H_2 molecular gas obtained from NaCo are shown in blue. **Bottom right:** *Chandra* X-ray image in the 0.5-7 keV band with the same FoV as the previous panel. The contours of the warm H_2 molecular gas obtained from NaCo are shown in blue. colour scales are linear and in arbitrary units. North is up and east is to the left.

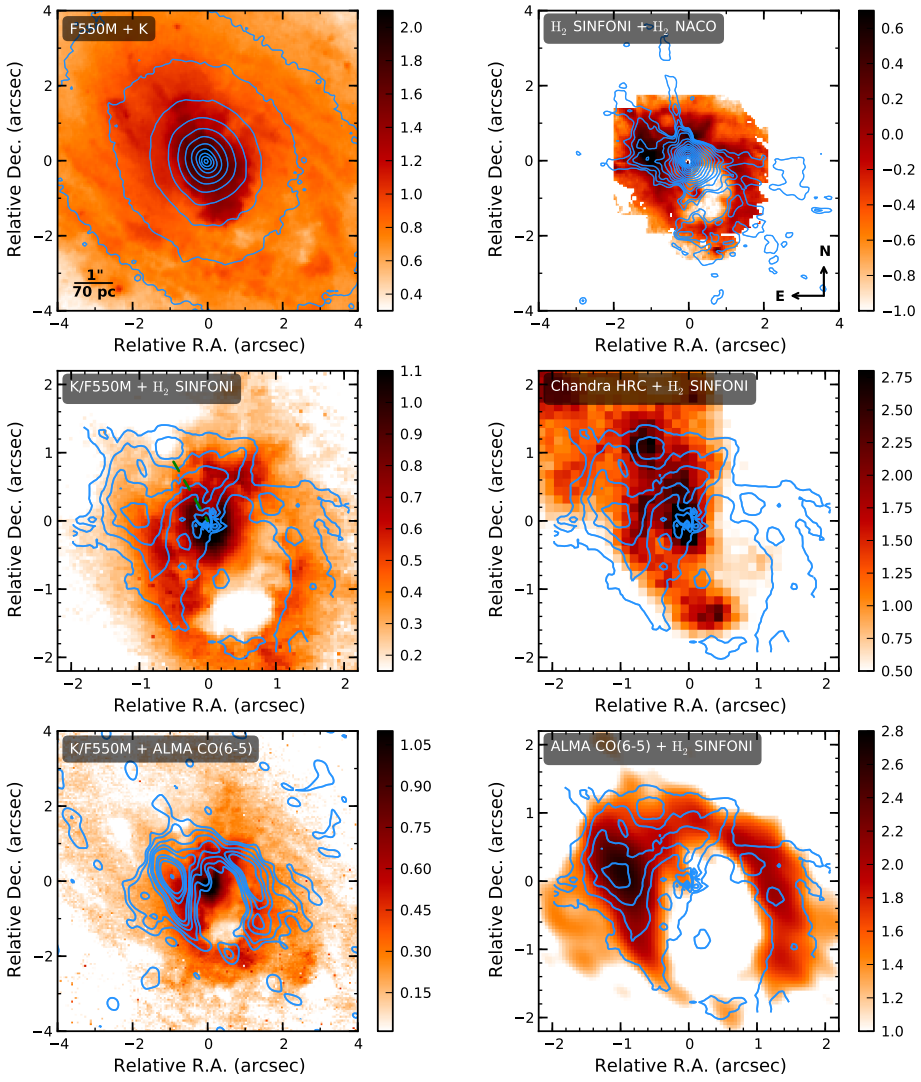

Figure 5. NGC 1068. **Top left**: *HST/F550M* image with NaCo/*K*-band continuum contours in blue. The FoV is 8 arcsec × 8 arcsec. **Top right:** Intensity map of the warm H_2 molecular gas obtained from IFU SINFONI (from Müller Sánchez et al. 2009). The FoV is the same as the previous panel. The contours of the warm H_2 molecular gas obtained from NaCo are shown in blue. They start at three times the background noise level and increase in factors of 3. **Middle left:** *K/F550M* ratio or dust map with a FoV of 4.4 arcsec × 4.4 arcsec. The contours of the warm H_2 molecular gas obtained from IFU SINFONI are shown in blue. The orientation of the radio jet (e.g. Gallimore et al. 1996) is indicated with a dashed green line. **Middle right:** *Chandra* HRC image from Wang et al. (2012) with the same FoV as the previous panel. The contours of the warm H_2 molecular gas obtained from SINFONI are shown in blue. **Bottom left:** *K/F550M* ratio or dust map with a FoV of 8 arcsec × 8 arcsec. The contours of the CO(6-5) molecular gas obtained from ALMA (García-Burillo et al. 2014) are shown in blue. Contours levels go from 5σ to 240σ, where σ = 2 Jy beam^{-1} km s^{-1} (García-Burillo et al. 2014). **Bottom right:** ALMA CO(6-5) integrated intensity map (from García-Burillo et al. 2014) with a FoV of 4.4 arcsec × 4.4 arcsec. The contours of the warm H_2 molecular gas obtained from SINFONI are shown in blue. The colour scale is logarithmic in 0.87 Jy beam^{-1} km s^{-1}. The colour palettes in the other panels are logarithmic and in arbitrary units. North is up and east is to the left.

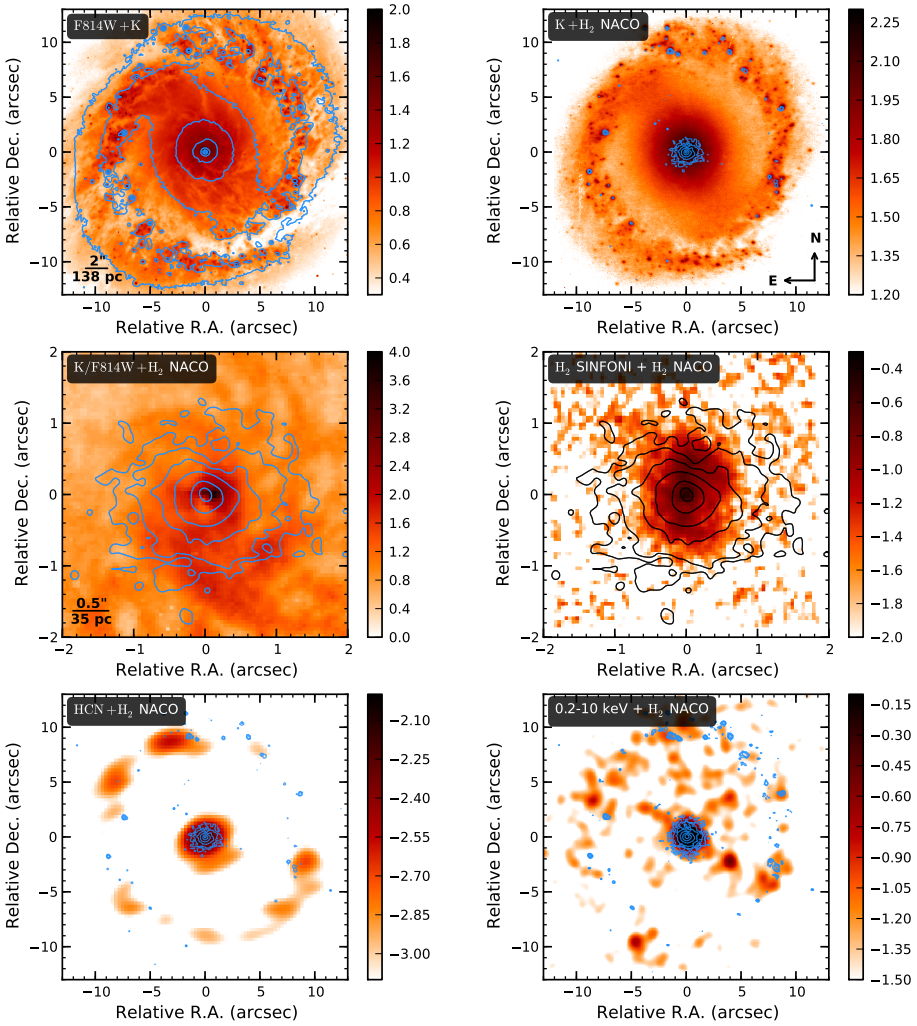

Figure 6. NGC 1097. **Top left**: *HST/F814W* image with NaCo/*K*-band continuum contours in blue. The FoV is 26 arcsec × 26 arcsec. **Top right:** NaCo/*K*-band image with the same FoV as the previous panel. The contours of the warm H_2 molecular gas obtained from NaCo are shown in blue. They start at three times the background noise level and increase in factors of 2. **Middle left:** *K/F814W* ratio or dust map with a FoV of 4 arcsec × 4 arcsec. The contours of the warm H_2 molecular gas obtained from NaCo are shown in blue. **Middle right:** Intensity map of the warm H_2 molecular gas obtained from IFU SINFONI. The FoV is the same as the previous panel. The contours of the warm H_2 molecular gas obtained from NaCo are shown in black. **Bottom left:** HCN image with a FoV of 26 arcsec × 26 arcsec. The contours of the warm H_2 molecular gas obtained from NaCo are shown in blue. **Bottom right:** *Chandra* X-ray image in the 0.2-10 keV band with the same FoV as the previous panel. The contours of the warm H_2 molecular gas obtained from NaCo are shown in blue. colour scales are logarithmic and in arbitrary units. North is up and east is to the left.

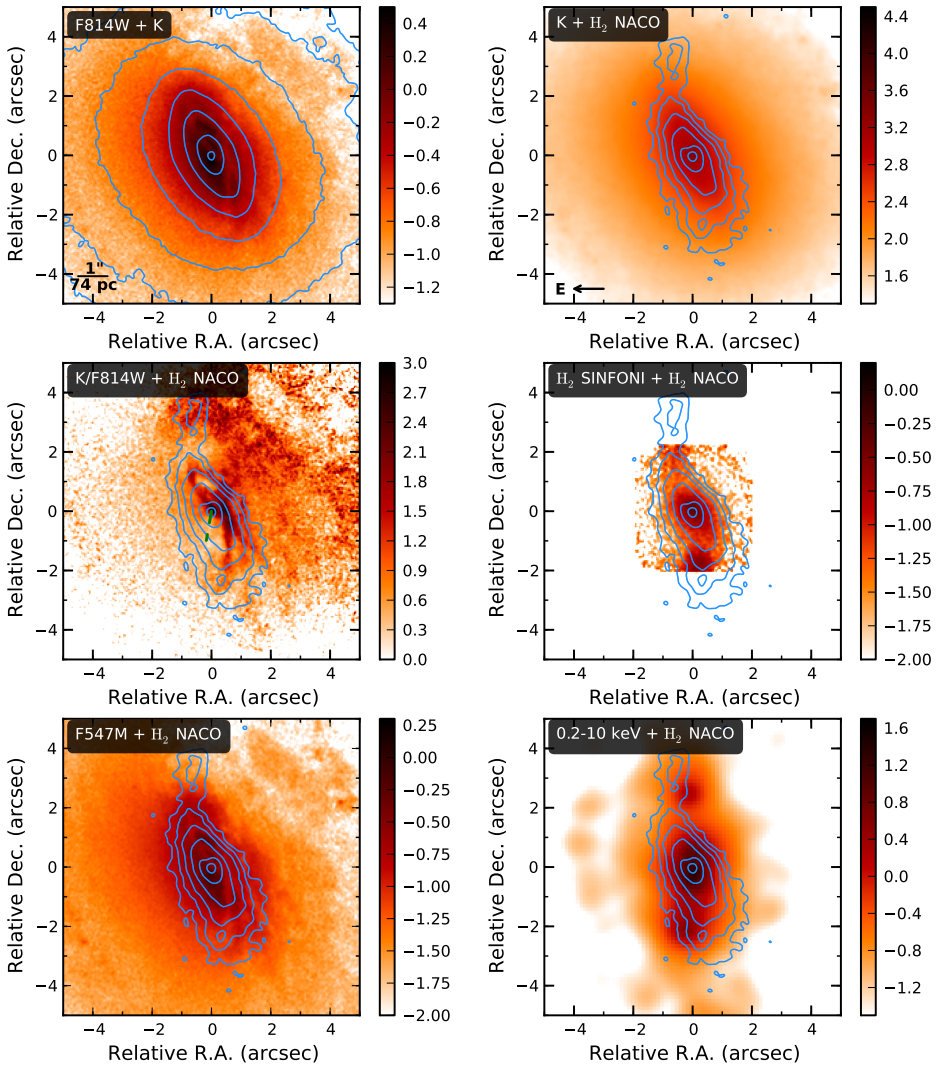

Figure 7. NGC 1386. **Top left**: *HST/F814W* image with NaCo/*K*-band continuum contours in blue. **Top right:**NaCo/*K*-band image. The contours of the warm H_2 molecular gas obtained from NaCo are shown in blue. They start at three times the background noise level and increase in factors of 2. **Middle left:** *K/F814W* ratio or dust map. The contours of the warm H_2 molecular gas obtained from NaCo are shown in blue. The orientation of the radio jet (e.g. Nagar & Wilson 1999) is indicated with a dashed green line. **Middle right:** Intensity map of the warm H_2 molecular gas obtained from IFU SINFONI. The contours of the warm H_2 molecular gas obtained from NaCo are shown in blue. **Bottom left:** *HST/F547M* image. The contours of the warm H_2 molecular gas obtained from NaCo are shown in blue. **Bottom right:** *Chandra* X-ray image in the 0.2-10 keV band. The contours of the warm H_2 molecular gas obtained from NaCo are shown in blue. colour scales are logarithmic and in arbitrary units. The FoV for all panels is 10 arcsec × 10 arcsec. North is up and east is to the left.

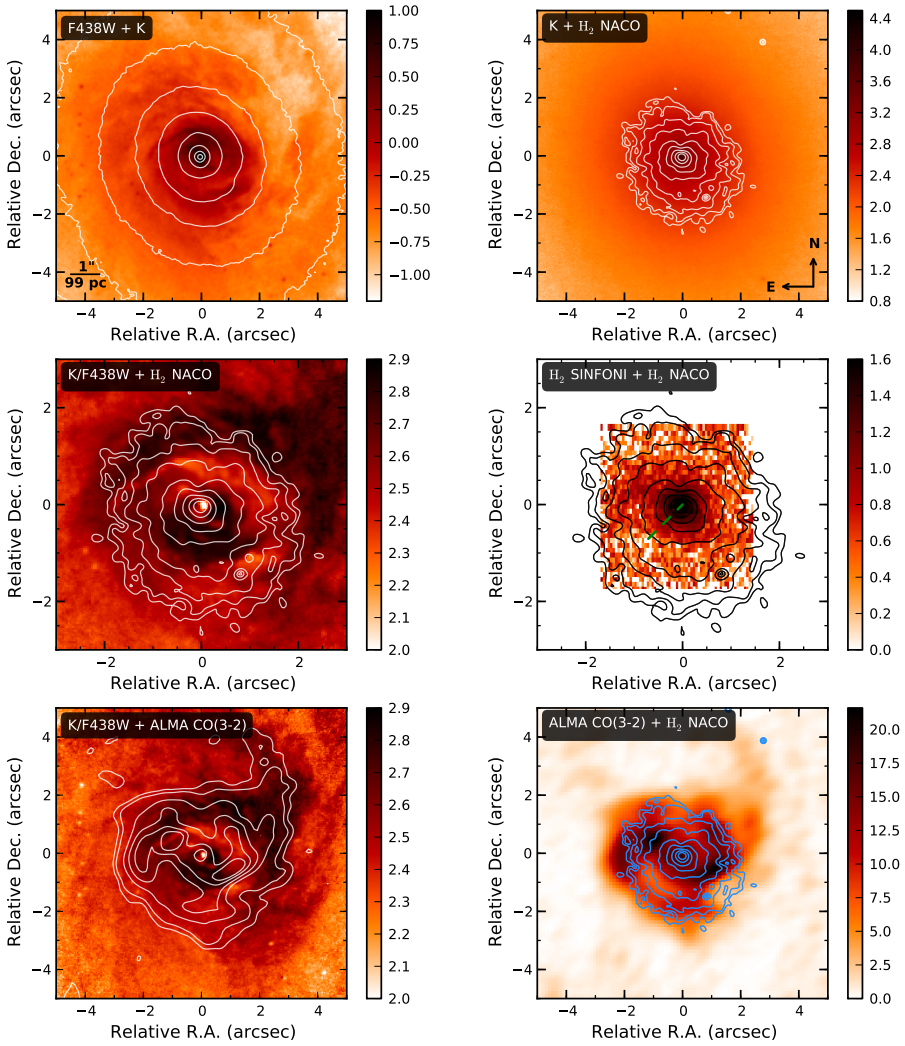

Figure 8. NGC 1566. **Top left**: *HST/F438W* image with NaCo/*K*-band continuum contours in white. The FoV is 10 arcsec × 10 arcsec. **Top right:**NaCo/*K*-band image with the same FoV as the previous panel. The contours of the warm H_2 molecular gas obtained from NaCo are shown in white. They start at three times the background noise level and increase in factors of 2. **Middle left:** *K/F438W* ratio or dust map with a FoV of 6 arcsec × 6 arcsec. The contours of the warm H_2 molecular gas obtained from NaCo are shown in white. **Middle right:** Intensity map of the warm H_2 molecular gas obtained from IFU SINFONI. The FoV is the same as the previous panel. The contours of the warm H_2 molecular gas obtained from NaCo are shown in black. The orientation of the narrow line region (e.g. Schmitt & Kinney 1996) is indicated with a dashed green line. **Bottom left:** *K/F438W* ratio or dust map with a FoV of 10 arcsec × 10 arcsec. The contours of the cold CO(3-2) molecular gas obtained from ALMA (Combes et al. 2014) are shown in white. Contours levels are 1.65, 2.7, 6.5, 10, 14 and 17 times 0.87 Jy beam^{-1} km s^{-1}. **Bottom right:** ALMA CO(3-2) integrated intensity map (from Combes et al. 2014) with the same FoV as the previous panel. The contours of the warm H_2 molecular gas obtained from NaCo are shown in blue. The colour scale is linear in 0.87 Jy beam^{-1} km s^{-1}. The colour palettes in the other panels are in arbitrary units. North is up and east is to the left.

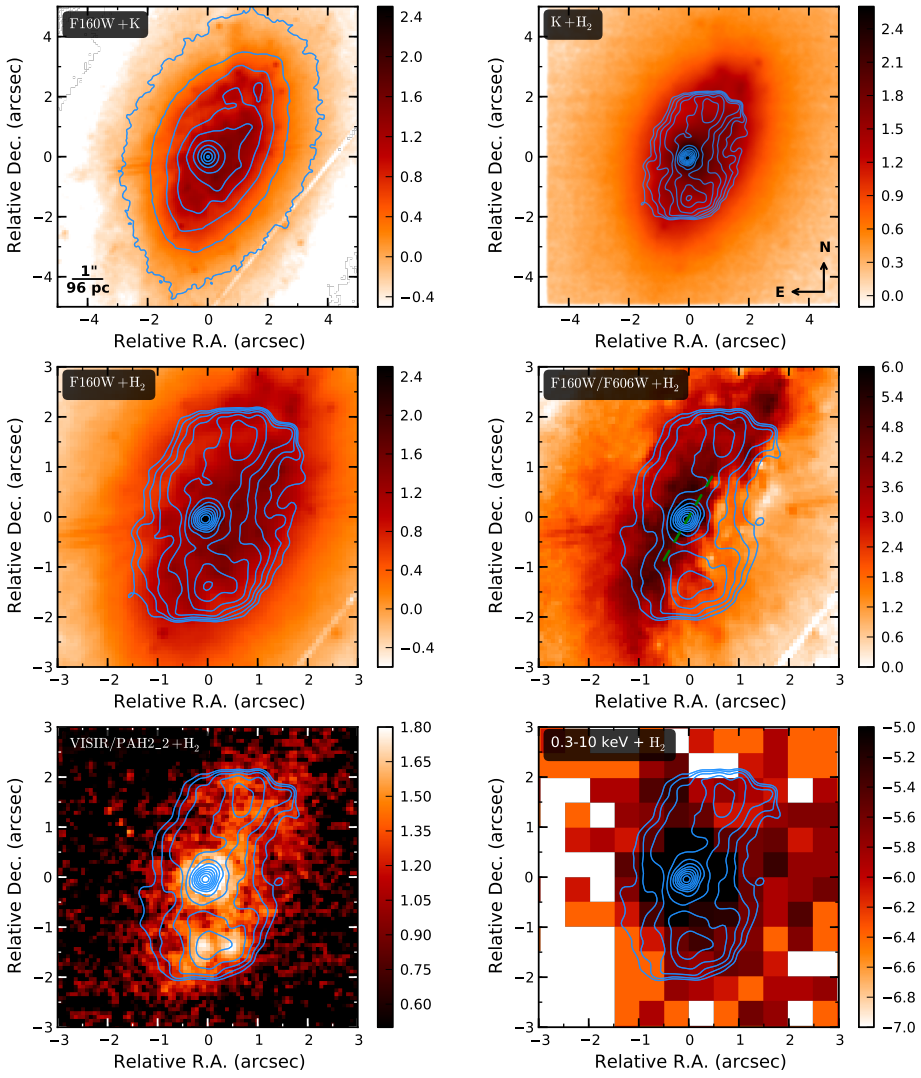

Figure 9. NGC 7582. **Top left**: *HST/F160W* image with NaCo/*K*-band continuum contours in blue. The FoV is 5 arcsec × 5 arcsec. **Top right:**NaCo/*K*-band image with the same FoV as the previous panel. The contours of the warm H_2 molecular gas obtained from IFU SINFONI are shown in blue. They start at three times the background noise level and increase in factors of 1.2. **Middle left:** *HST/F160W* image with a FoV of 6 arcsec × 6 arcsec. The contours of the warm H_2 molecular gas obtained from IFU SINFONI are shown in blue. **Middle right:** *F160W/F606W* ratio or dust map with the same FoV as the previous panel. The contours of the warm H_2 molecular gas obtained from IFU SINFONI are shown in blue. The orientation of the narrow line region (e.g. Ulvestad & Wilson 1984; Morganti et al. 1999) is indicated with a dashed green line. **Bottom left:** *VISIR/PAH2_2* image (11.88 μm) with the same FoV as the previous panels. The contours of the warm H_2 molecular gas obtained from IFU SINFONI are shown in blue. **Bottom right:** *Chandra* X-ray image in the 0.3-10 keV band with the same FoV as the previous panels. The contours of the warm H_2 molecular gas obtained from IFU SINFONI are shown in blue. colour scales are logarithmic and in arbitrary units. North is up and east is to the left.

APPENDIX A: DISCUSSION ON INDIVIDUAL OBJECTS

CenA

Centaurus A (also NGC5128 or CenA), at a distance of 3.8 ± 0.1 Mpc (Harris et al. 2010), is the most nearby elliptical galaxy and a merger archetype. It hosts a Sy2 nucleus, covered by a prominent dust lane (see Fig. 3, top left), that emits a powerful radio and X-ray jet up to kpc scales. The NaCo narrow-band imaging of CenA shows that the molecular H_2 gas is concentrated in a spherical nuclear region of radius ∼0.3 arcsec (∼5 pc; Fig. 3, top right panel). Further out, fainter shells of gas emission are traced up to ∼3 arcsec (∼50 pc) north-east and south of the nucleus. This extended morphology is in agreement with the overall distribution observed in the SINFONI map (Fig. 3, middle-right panel), where shell features are observed (Neumayer et al. 2007). These were interpreted as jet bow shocks, which is consistent with the orientation of the radio jet at pc scales (Fig. 3, middle-left panel). The warm H_2 gas distribution does not follow the filamentary dust morphology traced by the $K - I$ colour map nor the cold CO(2-1) gas emission (Espada et al. 2009; Espada 2013; Fig. 3, middle and bottom left panels). The nucleus and jet of CenA are the most likely heating sources that excite the H_2 molecules (Bicknell et al. 2013).

Circinus

At a distance of 4.2 ± 0.8 Mpc (Freeman et al. 1977), Circinus is one of the nearest Seyfert galaxies. It has a one-sided ionization cone north-west of the nucleus (Marconi et al. 1994; see also Fig. 4, middle-left panel). The nucleus of Circinus, which has been resolved by near-IR imaging (Prieto et al. 2004) and by interferometric observations at mid-IR (Tristram et al. 2014), is obscured at optical wavelengths (Prieto et al. 2004; Mezcua et al. in preparation).

The warm H_2 molecular gas emission is concentrated within a region of ∼2 arcsec (∼38 pc) radius, with the nuclear morphology in north-east-south-west direction (perpendicular to the ionization cone). This nuclear elongation is also observed in the small FoV of SINFONI presented by Müller Sánchez et al. (2006); see also Fig. 4, middle-right panel. The NaCo H_2 narrow-band image, with a larger FoV than SINFONI, reveals that extended H_2 emission in the form of ∼1 arcsec–wide arches is also detected ∼2 arcsec north-east and south-south-west of the nucleus. The northern spiral-like structure in the north-east curling turning towards west seems to be coincident with clumps of star formation in the I-band and Hα image (Fig. 4, bottom-left panel; Mezcua et al. in preparation), which suggests that the molecular gas in this region is heated by young stars, while the southern clumps seem to follow the spiral morphology of the dust colour map.

NGC 1068

The spiral SB galaxy NGC 1068, at a distance of 14.1 Mpc (Marco et al. 1997), hosts a very bright Sy2 nucleus that is obscured from optical wavelengths up to 1μm (e.g. Capetti et al. 1997; Prieto et al. 2010, 2014). The warm molecular H_2 gas distribution traced by NaCo covers a wider FoV than the SINFONI map and recovers the nuclear H_2 emission missing in the SINFONI map of Müller Sánchez et al. (2009) (nuclear hole in Fig. 5, upper right panel). It also shows clear diffraction effects (i.e. detector spikes) caused by the bright nucleus of this galaxy. Despite these diffraction effects and the nuclear differences, the extended NaCo morphology is consistent with that traced by SINFONI (e.g. Müller Sánchez et al. 2009, Barbosa et al. 2014; see also Galliano & Alloin 2002 for a VLT/ISAAC map): two prominent gas concentrations east and west of the nucleus and a collar-like structure south-west of it are observed on the NaCO map, similar to the SINFONI morphology and to the morphology of the slightly warm molecular gas (T ∼40–50 K) traced by recent CO(6-5) ALMA observations (García-Burillo et al. 2014) and which extends up to 2 arcsec (140 pc) from the nucleus (see Fig. 5, bottom-right panel).

Müller Sánchez et al. (2009) report the presence of a linear structure or northern tongue of H_2 emission streaming towards the nucleus. A good correlation between this northern tongue of H_2 gas and dust emission at 12μm was presented by these authors (also seen in the dust maps of Prieto et al. 2014), which provides further evidence that the tongue is transporting feeding material to the AGN (Tomono et al. 2006; though see Barbosa et al. 2014 for an outflow scenario). The superposition of the warm H_2 gas contours on the $V - K$ colour dust map (Fig. 5, middle-left panel) shows that the warm molecular gas is not only coincident with dust emission in the northern tongue but that an overall clear correlation is observed between the dust morphology and the H_2 emission, including the gas concentrations east and west of the nucleus and the ring-like structure ∼2 arcsec south of it. The correlation is however not one to one, as the warm H_2 gas presents a wider and more extended distribution than the dust. Despite the wider FoV of NaCo, no molecular H_2 gas emission is observed at scales larger than 2 arcsec, which indicates that all the warm molecular H_2 gas of NGC 1068 is concentrated in the central 140 pc.

In Section 4.4 we found that the X-ray emission is the most likely cause of excitation of the nuclear warm H_2 molecular gas for most sources. In some regions close to the strong nuclear X-ray source and devoid of dust the X-ray emission could be able not only to excite the H_2 molecules but even to dissociate them. This extreme case might be observed for NGC 1068, showcasing the role of dust in shielding H_2 molecules from the intense X-ray radiation: the south-west cavity seen in the dust map and H_2 contours (Fig. 5, middle-left panel) coincides with an excess of V-band (*HST/F550W*; Fig. 5, top-left panel) and *Chandra* emission (Fig. 5, middle-right panel), while the *Chandra* knot ∼1 arcsec north of the nucleus coincides with a depression in the dust map and a hole in the H_2 molecular gas distribution (Fig. 5, top-right panel); finally, an arch of X-ray *Chandra* emission ∼0.5 arcsec east of the nucleus is observed to coincide with an equivalent depression zone in the dust and H_2 gas maps. For NGC 1068 we might thus be seeing evidence that in the regions devoid of dust the H_2 molecule is not protected from the X-ray radiation but destroyed by it. This would explain the lack of H_2 emission in those regions where the X-ray emission is stronger, further supporting the existence of a clear link between H_2 molecular gas and X-ray radiation.

NGC 1097

NGC 1097 is a LINER/Sy1 galaxy located at 14.2 Mpc (Tully et al. 2009) with a prototypical nuclear ring (diameter ∼18 arcsec; ∼ 1.2 kpc). AO IR broad-band imaging by Prieto et al. (2005) revealed dusty spirals around the nucleus and reaching the star-forming ring.

The H_2 image of NGC 1097 (Fig. 6, top-right panel) is dominated by the nuclear emission, which can be traced up to 2 arcsec (∼ 140 pc) from the nucleus. Further out, in the star-forming ring at $r \simeq 8$ arcsec, several compact emission regions are detected.

These H_2 point sources are coincident with the stellar clusters in the K-band (Fig. 6, top-right panel; see also Prieto et al. 2005).

The nuclear H_2 emission shows a slightly elongated morphology along the east-west axis (middle-left panel in Fig. 6). This is in contrast with the H_2 1–0 S(1) intensity map obtained by Davies et al. (2009) with SINFONI (Fig. 6, middle-right panel), which shows a more compact morphology elongated along the north-south direction. The discrepancy is probably ascribed to the method used to estimate the continuum emission in Davies et al. (2009): the stellar and non-stellar continua are separated prior to the H_2 extraction, based on the dilution of the 2.3 μm CO band head. In order to accommodate the differences between both maps, the non-stellar emission should be also more extended along the north-south axis, but this is not observed neither in the *Ks*-band continuum nor in the $I-K$ colour map. The morphology of dust as traced by the $I-K$ colour (Fig. 6, middle-left panel) does in any case not correlate with the nuclear extent of the warm H_2 emission.

NGC 1386

NGC 1386 is a spiral Sb(s)a galaxy located in the Fornax cluster, at a distance of 15.3 Mpc (Jensen et al. 2003), that hosts a Sy2 nucleus. NGC 1386 has a star-forming ring with a diameter of 30 arcsec (2.2 kpc) and tightly collimated ionized gas in the *HST* [O III] and Hα images extending 2 arcsec–3 arcsec towards north and south from the optical nucleus (Ferruit et al. 2000; Prieto et al. 2014). It shows a one-sided jet oriented in the south-east direction (Nagar & Wilson 1999; Fig. 7, middle-left panel). The nucleus (or IR peak; Prieto et al. 2014) is obscured, located 0.23 arcsec north of the optical peak of emission.

The H_2 emission traced by NaCo presents a strong nuclear component and two extended regions up to 4 arcsec ($\sim$ 320 pc) towards the north and south of the nucleus (Fig. 7, top-right panel). The latter were reported by Reunanen et al. (2002) using long-slit spectroscopy in the near-IR. Its morphology, unveiled in this work for the first time, resembles that of the emission-line plumes detected in [O III] and [N II]+Hα by Ferruit et al. (2000). In the $I-K$ colour map (Fig. 7, middle-left panel), a dust lane is visible extending $\sim$ 3 arcsec towards north-east and south-west of the infrared nucleus. The peak of the H_2 emission is associated with the nucleus. The morphology of the extended H_2 emission resembles that of the dust lanes covering the IR nucleus, however it presents a much wider extent (middle-left panel in Fig. 7). No H_2 emission is detected in the star-forming ring.

NGC 1566

NGC 1566, at a distance of 20.5 Mpc (taken from NED adopting $H_0 = 73$ km s^{-1} Mpc^{-1}), is a nearly face-on SABbc spiral galaxy. It hosts a Seyfert nucleus that varies from type 1 to 2 (Alloin et al. 1985) and has a one-sided ionization cone detected in [O III] that extends 0.3 arcsec towards south-east (Schmitt & Kinney 1996); see also Fig. 8, middle-right panel. The optical *HST* images reveal dusty spirals reaching towards the nucleus (Malkan et al. 1998; see also dust map in Fig. 8, middle-left panel). Recent high-resolution CO ALMA observations show that the cold molecular CO(3-2) gas emission extends up to 3.5 arcsec forming a 2-arm nuclear spiral structure that corresponds very well with the dust lanes observed in the *HST* images (Combes et al. 2014) and the dust map in Fig. 8 (bottom-left panel) .

The NaCo warm H_2 molecular gas emission of NGC 1566 reveals an almost circular diffuse morphology (Fig. 8, top-right panel), slightly elongated in the east-west direction at $r < 1$ arcsec, similar to the H_2 emission detected by SINFONI (Fig. 8, middle-right panel). The extent of the warm H_2 gas region in the NaCo image is 2 arcsec ($\sim$220 pc), which is $\sim$2 times the size of that detected in the instrument-limited FoV of SINFONI and nearly the same as the extension of the H_2 emission detected by near-IR long-slit spectroscopy (Reunanen et al. 2002). The warm H_2 gas emission does not follow the dust spiral structure as does the CO emission (Fig. 8, bottom panels).

NGC 7582

NGC 7582 is a SBab galaxy located at 19.9 Mpc in the Grus Quartet (Terry et al. 2002). Its Sy2 nucleus, a strong IR source only seen from the *I*-band on (Prieto et al. 2014), is surrounded by star-forming clusters resolved in the nuclear starburst (Prieto et al. 2002; also visible in the *VISIR/PAH2_2* image (11.88 μm) in Fig. 9). The morphology of the warm H_2 gas emission, traced by SINFONI, extends up to 2 arcsec (192 pc) and is associated with the starburst emission. The most embedded clusters, detected in the mid-IR and radio wavelengths (Wold & Galliano 2006; Orienti & Prieto 2010), show a counterpart in the H_2 map (Fig. 9 bottom-left panel). A compact unresolved source of warm H_2 gas is detected at the position of the AGN and is most likely excited by X-ray emission (Fig. 9, bottom-right panel).